

Electronic Thesis and Dissertation Repository

8-24-2015 12:00 AM

Development of Glass Fiber Reinforced Poly(3-Hydroxybutyrate-co-3-Hydroxyhexanoate)

Willson Arifin, *The University of Western Ontario*

Supervisor: Takashi Kuboki, *The University of Western Ontario*

A thesis submitted in partial fulfillment of the requirements for the Master of Engineering Science degree in Mechanical and Materials Engineering

© Willson Arifin 2015

Follow this and additional works at: <https://ir.lib.uwo.ca/etd>



Part of the [Mechanical Engineering Commons](#)

Recommended Citation

Arifin, Willson, "Development of Glass Fiber Reinforced Poly(3-Hydroxybutyrate-co-3-Hydroxyhexanoate)" (2015). *Electronic Thesis and Dissertation Repository*. 3138.
<https://ir.lib.uwo.ca/etd/3138>

This Dissertation/Thesis is brought to you for free and open access by Scholarship@Western. It has been accepted for inclusion in Electronic Thesis and Dissertation Repository by an authorized administrator of Scholarship@Western. For more information, please contact wlsadmin@uwo.ca.

DEVELOPMENT OF GLASS FIBER REINFORCED POLY(3-
HYDROXYBUTYRATE-CO-3-HYDROXYHEXANOATE)

(Thesis format: Integrated Article)

by

Willson Arifin

Graduate Program in Mechanical and Materials Engineering

A thesis submitted in partial fulfillment
of the requirements for the degree of
Master of Engineering Science

The School of Graduate and Postdoctoral Studies
The University of Western Ontario
London, Ontario, Canada

© Willson Arifin 2015

Abstract

Enhancement of mechanical properties of the bacterial polyester poly(3-hydroxybutyrate-co-3-hydroxyhexanoate) (PHBH) by the addition of glass fibers (GF) and thermoplastic elastomers was investigated. Glass fiber addition significantly increased Young's modulus and strength of PHBH, but had little effect on the degree of crystallinity of PHBH. To increase ductility and/or energy absorbed in fracture, that were found to be reduced, in glass fiber reinforced PHBH composites, two types of thermoplastic elastomers, styrene-ethylene-butylene-styrene copolymer (SEBS) and maleated styrene-ethylene-butylene-styrene copolymer (SEBS-MA), were added to PHBH/GF composites. SEBS-MA was more effective than SEBS in improving ductility, fracture energy, and notched Izod impact strength of PHBH/GF composites. Both SEBS and SEBS-MA addition decreased the degree of crystallinity of PHBH/GF composites. In conclusion, it was found that mechanical properties of PHBH can be tailored by the addition of glass fibers and thermoplastic elastomers; therefore, modulus, strength, and energy absorption in fracture of PHBH composites can be balanced.

Keywords

Poly(3-hydroxy-butyrate-co-3-hydroxyhexanoate), Glass fiber, Styrene-ethylene-butylene-styrene copolymer, Maleated styrene-ethylene-butylene-styrene copolymer, Mechanical property, Thermal property

Co-Authorship Statement

1.

Title: Effects of Glass Fibers on Mechanical and Thermal Properties of Poly(3-hydroxybutyrate-co-3-hydroxyhexanoate) (Chapter 2)

Authors: **Willson Arifin** and Takashi Kuboki

Willson Arifin collected, analyzed, and interpreted the data under the constructive suggestions of Dr. Takashi Kuboki. Willson Arifin drafted the manuscript under the guidance of Dr. Takashi Kuboki, and the manuscript was revised by Dr. Takashi Kuboki. This manuscript will be submitted for publication.

2.

Title: Effects of Thermoplastic Elastomers on Mechanical and Thermal Properties of Glass Fiber Reinforced Poly(3-hydroxybutyrate-co-3-hydroxyhexanoate) (Chapter 3)

Authors: **Willson Arifin** and Takashi Kuboki

Willson Arifin collected, analyzed, and interpreted the data under the constructive suggestions of Dr. Takashi Kuboki. Willson Arifin drafted the manuscript under the guidance of Dr. Takashi Kuboki, and the manuscript was revised by Dr. Takashi Kuboki. This manuscript will be submitted for publication.

Acknowledgments

First and foremost, I would like to sincerely thank my advisor, Dr. Takashi Kuboki, for his patience, guidance, technical support, and encouragement throughout this research process.

I am grateful to Dr. Jeff Wood for being in my advisory committee and Dr. Xueliang Sun, Dr. Remus Tutunea-Fatan, Dr. Wenxing Zhou for being my examiners.

I would like to thank Dr. Paul Charpentier for allowing me to access his laboratory facility to perform characterization tests used in this research. I would also like to thank Mr. Tim Goldhawk from the Western Nanofabrication facility for his assistance in using a scanning electron microscope.

I would like to thank the assistance from the faculty and staff members in the Department of Mechanical and Materials Engineering at The University of Western Ontario. I would also like to thank all of the students that had worked in our lab for their help and accompany.

I am also grateful to the generous donation of materials from Kaneka Corporation, Owens Corning, and Kraton polymers.

Finally, I would like to extend my sincere gratitude to my family and friends for their continuous support and encouragement.

Table of Contents

Abstract.....	ii
Co-Authorship Statement.....	iii
Acknowledgments.....	iv
Table of Contents.....	v
List of Tables.....	viii
List of Figures.....	ix
Chapter 1.....	1
1 Introduction.....	1
1.1 Background.....	1
1.2 Objective.....	4
1.3 Significance.....	4
1.4 Thesis Outline.....	5
1.5 References.....	6
Chapter 2.....	11
2 Effects of Glass Fiber on Mechanical and Thermal Properties of Poly(3-hydroxybutyrate-co-3-hydroxyhexanoate).....	11
2.1 Introduction.....	11
2.2 Experimental.....	13
2.2.1 Materials.....	13
2.2.2 Fabrication of composites.....	13
2.2.3 Measurement of fiber length.....	14
2.2.4 Characterization of mechanical properties.....	16
2.2.5 Characterization of thermal properties.....	16
2.3 Result and Discussion.....	17

2.3.1	Fiber length frequency distribution and average fiber length.....	17
2.3.2	Mechanical properties.....	20
2.3.3	Prediction of Young's modulus	24
2.3.4	Prediction of strength.....	26
2.3.5	Thermal properties	33
2.3.6	Non-isothermal crystallization kinetics	38
2.4	Conclusion	42
2.5	Reference	42
Chapter 3.....		49
3	Effects of Thermoplastic Elastomers on Mechanical and Thermal Properties of Glass Fiber Reinforced Poly(3-hydroxybutyrate-co-3-hydroxyhexanoate)	49
3.1	Introduction.....	49
3.2	Experimental.....	51
3.2.1	Materials	51
3.2.2	Fabrication of composites.....	52
3.2.3	Measurement of fiber length.....	52
3.2.4	Characterization of mechanical properties.....	53
3.2.5	Observation of fracture surface.....	54
3.2.6	Characterization of thermal properties.....	54
3.3	Results and Discussion	54
3.3.1	Fiber length frequency distribution and average fiber length.....	54
3.3.2	Tensile properties.....	60
3.3.3	Notched Izod impact strength	68
3.3.4	Thermal properties	73
3.3.5	Non-isothermal crystallization kinetics	78
3.4	Conclusions.....	82

3.5 Reference	83
Chapter 4.....	90
4 Conclusions and Recommendations for Future Study.....	90
4.1 Conclusions.....	90
4.2 Recommendations for Future Study	92
Curriculum Vitae	94

List of Tables

Table 2.1 Information on composite materials prepared in this study.....	15
Table 2.2 Properties of PHBH and glass fiber used for predictions	16
Table 2.3 Thermal properties of PHBH5.6 and PHBH11.1 composites characterized from the first DSC curves	36
Table 2.4 Thermal properties of PHBH5.6 and PHBH11.1 composites characterized from the second DSC heating curves	37
Table 2.5 Thermal properties of PHBH5.6 composites characterized from the DSC cooling curves and non-isothermal kinetic parameters calculated from the modified Avrami equation	41
Table 3.1 Information on composite materials prepared in this study.....	53
Table 3.2 Thermal properties of PHBH/GF/TE composites characterized from the first DSC curves	76
Table 3.3 Thermal properties of PHBH/GF/TE composites characterized from the second DSC heating curves.....	77
Table 3.4 Thermal properties of PHBH5.6/GF/TE composites characterized from the DSC cooling curves and non-isothermal kinetic parameters calculated from the modified Avrami equation.....	81

List of Figures

Figure 2.1 Fiber length frequency distribution for PHBH5.6 with (a) 5 vol% and (b) 23 vol% fibers as well as PHBH11.1 with (c) 5 vol% and (d) 23 vol% fibers	18
Figure 2.2 Average length of fibers in the injection-molded composite specimen versus the volume fraction of fiber	19
Figure 2.3 Torque versus time for (a) PHBH5.6 and (b) PHBH11.1 composites	20
Figure 2.4 Stress-strain curves of (a) PHBH5.6 and (b) PHBH11.1 composites	21
Figure 2.5 Mechanical properties of PHBH5.6 and PHBH11.1 composites: (a) Young's modulus, (b) Strength, (c) Strain at failure, and (d) Fracture energy.....	23
Figure 2.6 Young's modulus predicted by Halpin-Tsai and Tsai-Pagano equations for (a) PHBH5.6 and (b) PHBH11.1 composites.....	26
Figure 2.7 Interfacial shear stress of PHBH5.6 and PHBH11.1 composites.....	30
Figure 2.8 Fiber orientation factor of PHBH5.6 and PHBH11.1 composites.....	31
Figure 2.9 Strength predicted by the Bowyer-Bader method for (a) PHBH5.6 and (b) PHBH11.1 composites.....	32
Figure 2.10 First DSC heating curves of (a) PHBH5.6 and (b) PHBH11.1 composites	34
Figure 2.11 Second DSC heating curves of (a) PHBH5.6 and (b) PHBH11.1 composites....	34
Figure 2.12 DSC cooling curves of (a) PHBH5.6 and (b) PHBH11.1 composites	38

Figure 2.13 Avrami plots of PHBH5.6 composites	41
Figure 3.1 Fiber length frequency distribution for PHBH5.6/GF composites with (a) no thermoplastic elastomers, (b) SEBS, and (c) SEBS-MA.....	56
Figure 3.2 Fiber length frequency distribution for PHBH11.1/GF composites with (a) no thermoplastic elastomers, (b) SEBS, and (c) SEBS-MA.....	57
Figure 3.3 Average length of fibers in the injection-molded composite specimens.....	58
Figure 3.4 Torque versus time for (a) PHBH5.6/GF-based composites and (b) PHBH11.1/GF-based composites at the extruder barrel temperature of 150°C	58
Figure 3.5 Torque versus time for SEBS and SEBS-MA at the extruder barrel temperature of 220°C	59
Figure 3.6 Stress-strain curves of (a) PHBH5.6/GF-based composites and (b) PHBH11.1/GF-based composites	60
Figure 3.7 Mechanical properties of PHBH/GF composites without thermoplastic elastomers, with SEBS, and with SEBS-MA: (a) Young's modulus, (b) Strength, and (c) Strain at failure	62
Figure 3.8 Photographs of PHBH/GF composite specimens after tensile tests under transmitted light	64
Figure 3.9 Fracture energy of PHBH/GF composites without thermoplastic elastomers, with SEBS, and with SEBS-MA.....	65

Figure 3.10 SEM images of fracture surface of PHBH/GF composite specimens after tensile test.....	66
Figure 3.11 Notched Izod impact strength of PHBH/GF composites without thermoplastic elastomers, with SEBS, and with SEBS-MA.....	68
Figure 3.12 Photographs of PHBH/GF composite specimens after notched Izod impact tests under transmitted light	70
Figure 3.13 SEM images of fracture surface of PHBH/GF composites after notched Izod impact tests.....	71
Figure 3.14 First DSC heating curves of (a) PHBH5.6/GF-based composites and (b) PHBH11.1/GF-based composites	74
Figure 3.15 Second DSC heating curves of (a) PHBH5.6/GF-based composites and (b) PHBH11.1/GF-based composites	74
Figure 3.16 DSC cooling curves of (a) PHBH5.6/GF-based composites and (b) PHBH11.1/GF-based composites	78
Figure 3.17 Avrami plots of PHBH5.6/GF-based composites	81

Chapter 1

1 Introduction

1.1 Background

Plastics have become the most common engineering materials due to their low density, good processability, and good corrosion resistance [1]. In 2013, worldwide annual production of plastics reached 300 million tons [2], resulting in substantial petroleum usage [3]. This problem can be alleviated using biopolymers. Biopolymers are derived from biological sources, including starch, cellulose, fatty acids, sugars, proteins, and other sources. Some examples of biopolymers are polyhydroxyalkanoates (PHAs), polylactic acid (PLA), poly(butylene succinate) (PBS), and poly(propylene carbonate) (PPC). These polymers are known to be sustainable, environmentally friendly, and less petroleum dependent than synthetic polymers [4].

Among the biopolymers, PHAs, which are used in packaging [5,6] and medical applications [5–8], have received considerable attention [5,9]. PHAs are thermoplastic polyesters and are a family of polymers synthesized completely using biological processes, with carbon sources converted directly into PHAs by microbial fermentation [10–13]. PHAs biodegrade into carbon dioxide and water [14] and, during production, they consume less energy and emit less carbon dioxide than synthetic polymers [15]. Although many different types of PHAs have been reported [16], the most common PHA is the homopolymer poly(3-hydroxybutyrate) (PHB). PHB is brittle, due to its high

crystallinity, and has a high melting temperature of about 180°C [11,17], resulting in its processing temperature having to be at least 190°C. At this temperature, however, thermal degradation proceeds rapidly [18–20]. Therefore, it is difficult to manufacture PHB products through melt processes such as extrusion and injection molding.

Properties of PHB can be modified by introducing a comonomer and, thus, changing its content [17,21]. For example, the comonomer 3-hydroxyvalerate (3HV) has been introduced into PHB to form its most popular copolymer, poly(3-hydroxybutyrate-co-3-hydroxyvalerate) (PHBV). The copolymerization mitigated the problems mentioned above to some extent. However, PHBV is still brittle and not well suited for some industrial applications, such as films for deep drawing articles or injection molding [22].

Poly(3-hydroxybutyrate-co-3-hydroxyhexanoate) (PHBH) is another copolymer of PHB. The addition of its 3-hydroxyhexanoate (3HH) unit broadens process temperature as well as increases ductility, but decreases modulus and strength [14,23,24]. Although PHBH shows better ductility and processability than PHB and PHBV, further improvement of its mechanical properties and processability is desired to expand its possible applications.

One way to improve mechanical properties of polymers is to add fibers to form composite materials. Composite materials often have high stiffness- and high strength-to-weight ratios [25,26]. These advantages allow manufacturers to design components with low weight. Composite materials can be classified according to fiber length: long fiber reinforced composites and short fiber reinforced composites. In general, long fiber reinforced composites possess better mechanical properties due to their high aspect ratio of fiber. On the other hand, short fiber reinforced composites offer better processability.

Short fibers can be easily mixed with the polymer matrix, and the polymer/fiber mixture can be processed using industry-friendly polymer processing equipment, such as extrusion and injection molding, to produce parts with complex shapes [27].

In addition to length, fibers vary in composition, leading to options such as glass fibers, carbon fibers, and aramid fibers. Glass fibers are currently widely used to reinforce polymers due to their low cost, high tensile strength, high chemical resistance, and excellent insulating properties [28,29]. Carbon fibers are popular in aerospace and military applications due to their high specific tensile strength and modulus, low thermal expansion, high thermal conductivity, and high temperature resistance. Despite their excellent properties, the high cost of carbon fibers has excluded them from widespread commercial applications. Aramid fibers are also popular fibers and have higher specific strength and ductility [30] than glass or carbon fibers [27]. They are widely used in marine and aerospace applications where low weight, high tensile strength, and resistance to impact damage are important [28]. One of the major disadvantages of aramid fibers is difficulty in cutting and machining them [1,28]. Taking into account advantages and disadvantages of different fibers, in this study, short glass fibers were used to reinforce PHBH.

One of the important issues related to processability of PHBH is its crystallization. Because 3HH units are excluded from the PHB lattice during the crystallization of PHBH, the addition of 3HH decreases the crystallization rate and the degree of crystallinity of PHB [23]. Slow crystallization results in long molding-cycle time, thus leading to low productivity and high energy consumption in industrial processing. Furthermore, low degree of crystallinity can give rise to low modulus and strength of

final products. Therefore, it is important to investigate whether the crystallization rate and the degree of crystallinity of PHBH changes when additives (e.g., fibers, fillers, and polymers) are mixed with PHBH.

1.2 Objective

The main objective of this study is to manufacture glass fiber reinforced PHBH composites using industry-friendly polymer processing equipment, and to explore ways of tailoring their physical properties. Specific work included:

(1) increasing Young's modulus and tensile strength of PHBH using glass fibers (GF), and

(2) increasing ductility and energy absorption in fracture of PHBH/GF composites using thermoplastic elastomers (TE).

1.3 Significance

At this moment, no study has yet reported on PHBH/GF composites or its hybrid composites with TE. PHBH/GF/TE hybrid composites with a wide range of mechanical properties have many potential applications. Furthermore, most previous studies of PHBH used thin film casting with solvents, whereas, in this study, PHBH/GF/TE hybrid composites were manufactured by melt-compounding and injection molding. This melt processing is more industry-friendly and enables the production of a large number of 3D products. The research outcome will assist plastic and composite manufacturers in developing PHBH/GF/TE hybrid composite products.

1.4 Thesis Outline

This thesis is prepared in an Integrated-Article format as specified by the School of Graduate and Postdoctoral Studies at Western University, London, Ontario, Canada. This thesis consists of four chapters:

Chapter 1 presents a general background, objective, significance, and thesis outline.

In Chapter 2, the effects of glass fiber on the mechanical properties of PHBH are investigated. Preparation of PHBH composites by melt-compounding and injection molding, using two types of PHBH and short glass fiber content varying from 0 to 23 volume percent, is described. Tensile properties of PHBH composites are compared with mathematical models. The Halpin-Tsai and Tsai-Pagano equations are used to predict Young's modulus of PHBH composites, and the modified Kelly-Tyson model with the Bowyer-Bader method are used for strength prediction. The effects of glass fiber on the thermal properties of PHBH are also studied. The thermal properties include cold crystallization temperature, melting temperatures, crystallization temperature, degree of crystallinity, and crystallization half-time.

In Chapter 3, the effects of thermoplastic elastomers on the mechanical properties of glass fiber reinforced PHBH composites are studied. The thermoplastic elastomers used are styrene-ethylene-butylene-styrene copolymer (SEBS) and maleated styrene-ethylene-butylene-styrene copolymer (SEBS-MA). Mechanical properties are evaluated using tensile tests and notched Izod impact tests. The morphologies of PHBH/GF/TE hybrid composites are examined, and relationships between morphology and mechanical

properties are discussed. Furthermore, the effects of thermoplastic elastomers on the thermal properties of PHBH are studied.

Chapter 4 summarizes and concludes the thesis and provides recommendations for future study.

1.5 References

- [1] Mazumdar SK. *Composite Manufacturing: Materials, Product, and Process Engineering*. CRC Press; 2001.
- [2] PlasticsEurope. *Production of Plastics Worldwide from 1950 to 2013 (in Million Metric Tons)*. 2015.
- [3] Halden RU. Plastics and health risks. *Annu Rev Public Health* 2010;31:179–94. doi:10.1146/annurev.publhealth.012809.103714.
- [4] Chen G-Q, Patel MK. Plastics derived from biological sources: present and future: a technical and environmental review. *Chem Rev* 2012;112:2082–99. doi:10.1021/cr200162d.
- [5] Philip S, Keshavarz T, Roy I. Polyhydroxyalkanoates: biodegradable polymers with a range of applications. *J Chem Technol Biotechnol* 2007;82:233–47. doi:10.1002/jctb.1667.
- [6] Chen G-Q. A microbial polyhydroxyalkanoates (PHA) based bio- and materials industry. *Chem Soc Rev* 2009;38:2434–46.

- [7] Williams SF, Martin DP, Horowitz DM, Peoples OP. PHA applications: addressing the price performance issue. *Int J Biol Macromol* 1999;25:111–21. doi:10.1016/S0141-8130(99)00022-7.
- [8] Chen G-Q, Wu Q. The application of polyhydroxyalkanoates as tissue engineering materials. *Biomaterials* 2005;26:6565–78. doi:10.1016/j.biomaterials.2005.04.036.
- [9] Du C, Sabirova J, Soetaert W, Ki Carol Lin S. Polyhydroxyalkanoates production from low-cost sustainable raw materials. *Curr Chem Biol* 2012;6:14–25.
- [10] Anderson AJ, Dawes EA. Occurrence, metabolism, metabolic role, and industrial uses of bacterial polyhydroxyalkanoates. *Microbiol Rev* 1990;54:450–72.
- [11] Lee SY. Bacterial polyhydroxyalkanoates. *Biotechnol Bioeng* 1996;49:1–14. doi:10.1002/(SICI)1097-0290(19960105)49:1<1::AID-BIT1>3.0.CO;2-P.
- [12] Madison LL, Huisman GW. Metabolic Engineering of Poly(3-Hydroxyalkanoates): From DNA to Plastic. *Microbiol Mol Biol Rev* 1999;63:21–53.
- [13] Wang Y, Yin J, Chen G-Q. Polyhydroxyalkanoates, challenges and opportunities. *Curr Opin Biotechnol* 2014;30:59–65. doi:10.1016/j.copbio.2014.06.001.
- [14] Asrar J, Valentin HE, Berger PA, Tran M, Padgett SR, Garbow JR. Biosynthesis and properties of poly(3-hydroxybutyrate-co-3-hydroxyhexanoate) polymers. *Biomacromolecules* 2002;3:1006–12. doi:10.1021/bm025543a.

- [15] Akiyama M, Tsuge T, Doi Y. Environmental life cycle comparison of polyhydroxyalkanoates produced from renewable carbon resources by bacterial fermentation. *Polym Degrad Stab* 2003;80:183–94. doi:10.1016/S0141-3910(02)00400-7.
- [16] Steinbüchel A, Valentin HE. Diversity of bacterial polyhydroxyalkanoic acids. *FEMS Microbiol Lett* 1995;128:219–28. doi:10.1111/j.1574-6968.1995.tb07528.x.
- [17] Laycock B, Halley P, Pratt S, Werker A, Lant P. The chemomechanical properties of microbial polyhydroxyalkanoates. *Prog Polym Sci* 2013;38:536–83. doi:10.1016/j.progpolymsci.2012.06.003.
- [18] Janigová I, Lacík I, Chodák I. Thermal degradation of plasticized poly(3-hydroxybutyrate) investigated by DSC. *Polym Degrad Stab* 2002;77:35–41. doi:http://dx.doi.org/10.1016/S0141-3910(02)00077-0.
- [19] Grassie N, Murray EJ, Holmes PA. The thermal degradation of poly(-(d)- β -hydroxybutyric acid): Part 2—Changes in molecular weight. *Polym Degrad Stab* 1984;6:95–103. doi:10.1016/0141-3910(84)90075-2.
- [20] Grassie N, Murray EJ, Holmes PA. The thermal degradation of poly(-(d)- β -hydroxybutyric acid): Part 3—The reaction mechanism. *Polym Degrad Stab* 1984;6:127–34. doi:10.1016/0141-3910(84)90032-6.
- [21] Sudesh K, Abe H, Doi Y. Synthesis, structure and properties of polyhydroxyalkanoates: biological polyesters. *Prog Polym Sci* 2000;25:1503–55. doi:10.1016/S0079-6700(00)00035-6.

- [22] El-Hadi A, Schnabel R, Straube E, Müller G, Henning S. Correlation between degree of crystallinity, morphology, glass temperature, mechanical properties and biodegradation of poly (3-hydroxyalkanoate) PHAs and their blends. *Polym Test* 2002;21:665–74. doi:10.1016/S0142-9418(01)00142-8.
- [23] Doi Y, Kitamura S, Abe H. Microbial Synthesis and Characterization of Poly(3-hydroxybutyrate-co-3-hydroxyhexanoate). *Macromolecules* 1995;28:4822–8. doi:10.1021/ma00118a007.
- [24] Alata H, Aoyama T, Inoue Y. Effect of Aging on the Mechanical Properties of Poly(3-hydroxybutyrate- co -3-hydroxyhexanoate). *Macromolecules* 2007;40:4546–51. doi:10.1021/ma070418i.
- [25] Khanam PN, Khalil HPSA, Jawaid M, Reddy GR, Narayana CS, Naidu SV. Sisal/Carbon Fibre Reinforced Hybrid Composites: Tensile, Flexural and Chemical Resistance Properties. *J Polym Environ* 2010;18:727–33. doi:10.1007/s10924-010-0210-3.
- [26] Eann P. *Composite Materials and Joining Technologies for Composites*. New York: Springer; 2013.
- [27] Gibson RF. *Principles of Composite Material Mechanics, Third Edition*. CRC Press; 2011.
- [28] Malick PK. *Fiber-Reinforced Composites Materials, Manufacturing, and Design, Third Edition*. CRC Press; 2008.

- [29] Brigante D. *New Composite Materials: Selection, Design, and Application*. Springer; 2014.
- [30] Chawla KK. *Composite Materials: Science and Engineering*. 3rd ed. New York: Springer Berlin Heidelberg; 2012.

Chapter 2

2 Effects of Glass Fiber on Mechanical and Thermal Properties of Poly(3-hydroxybutyrate-co-3-hydroxyhexanoate)

2.1 Introduction

Polymers from renewable resources have been drawing a lot of interest over the past decades, mainly for two reasons, the first being environmental concerns and the second being the realization that our petroleum resources are finite. In general, polymers from renewable resources can be classified into three groups: natural polymers, such as starch, protein, and cellulose; synthetic polymers from bio-derived monomers, such as poly(lactic acid) (PLA); and polymers from microbial fermentation, such as poly(hydroxyalkanoates) (PHAs) [1].

PHAs are commonly used in the packaging [2,3] and medical [2,3] fields (especially in tissue engineering [4,5]). PHAs are biodegradable and biocompatible, and their properties can be tailored by changing comonomer units, average molecular weight, and molecular weight distribution [6,7]. Although many different types of PHAs have been reported [8], the homopolymer poly(3-hydroxybutyrate) (PHB) and its copolymer, poly(3-hydroxybutyrate-co-3-hydroxyvalerate) (PHBV), are the most popular types of PHAs. PHB is brittle, due to its high degree of crystallinity, and has a narrow processing temperature window because its melting and degradation temperatures are relatively

close [9–11]. Therefore, a comonomer, 3-hydroxyvalerate (3HV), has been introduced into PHB to form a copolymer, poly(3-hydroxybutyrate-co-3-hydroxyvalerate) (PHBV). The copolymerization mitigated the problems to some extent.

Poly(3-hydroxybutyrate-co-3-hydroxyhexanoate) (PHBH) is another copolymer of PHB. The addition of the 3-hydroxyhexanoate (3HH) unit broadens process temperature as well as increases ductility, but decreases modulus and strength [12–14]. Therefore, a current goal is to improve modulus and strength of PHBH.

As is the case with most polymers from petroleum, polymers from renewable resources are rarely used alone. Addition of fiber is one way to improve the mechanical properties of polymers from renewable resources. In particular, short fiber is of great interest because of its ease of processing and greater possibility to obtain complex shapes [15]. Although various types of short fibers are available, glass fibers are the most commonly used owing to their higher strength, stiffness, and ease of production. Previous studies found that the addition of short glass fiber improved mechanical properties of polymers from renewable resources such as poly(lactic acid) [16,17] and poly(3-hydroxybutyrate-co-4-hydroxybutyrate) [18].

In this study, glass fiber was added to improve mechanical properties, in particular Young's modulus and strength, of PHBH. The tensile properties of glass fiber reinforced PHBH composites were evaluated as a function of glass fiber content. To the authors' knowledge, there have been no previous reports on glass fiber reinforced PHBH composites. Furthermore, most previous studies of PHBH used thin film casting method with solvents [11,12,14,19–22]. In this study, PHBH composites were fabricated by melt-

compounding and injection molding. This melt processing is a more industry-friendly process and enables to produce a large number of 3D products, but it is more technically challenging because thermal degradation and solidification (including crystallization) of PHBH, as well as fiber breakage during the process, need to be taken into account. This study also investigated thermal properties, including crystallization kinetics, of glass fiber reinforced PHBH composites.

2.2 Experimental

2.2.1 Materials

The study used two types of PHBH, supplied by Kaneka Corporation. One type contained 5.6 mol% 3HH (named PHBH5.6) and had a weight-average molecular weight of 555,000 g/mol. The other type contained 11.1 mol% 3HH (named PHBH11.1) and had a weight-average molecular weight of 622,000 g/mol. The fibers used were chopped strand glass fibers (OCW-272, supplied by Owens Corning), with a diameter of 10 μm , a length ranging from 4 to 4.5 mm.

2.2.2 Fabrication of composites

PHBH was dried at 80°C using a convection oven to eliminate possible moisture. Composite samples were prepared using a mini-twin-screw extruder (HAAKE MiniLab). PHBH and fibers were compounded with conical co-rotating screws at 100 rpm for 10 minutes. The degree of fill in the extruder was set to 75% and barrel temperature was set to 150°C. The resulting molten composite was transferred to a preheated mini-injection molding machine (HAAKE MiniJet), which then injected the melt into a mold with a 120

bar injection pressure. Injection cylinder and mold temperatures were set to 150°C and 70°C, respectively. The injection-molded samples were stored at room temperature inside a re-sealable plastic bag for two days before testing. In this study, ten composite material types were prepared. Information on the composite materials is summarized in Table 2.1. Glass fiber contents were varied from 0 to 40 weight percent. Since volume fraction of material components is used to predict mechanical properties of composites, the weight fraction of fiber was converted to volume fraction of fiber, V_f , using equation 1.

$$V_f = \frac{W_f \rho_m}{W_f \rho_m + (1 - W_f) \rho_f} \quad (1)$$

where W_f is the weight fraction of fiber, ρ_m is polymer matrix density, and ρ_f is fiber density. The densities of the two types of PHBH and the glass fibers used in this study are listed in Table 2.2.

2.2.3 Measurement of fiber length

To measure length of glass fibers in an injection-molded specimen, PHBH in the composite specimen was burnt off in a convection oven at 600°C for 30 minutes. The leftover ash and fibers were dispersed in water to extract fibers. A few drops of fiber-water were then cast onto a glass slide. Fiber length was measured using an optical microscope (Laborlux 11 POL) equipped with a digital camera and imaging analysis software (Infinity Analyze). Lengths of about 1000 fibers were measured for each specimen. Based on the resulting data, fiber length frequency distribution and weighted average fiber length were obtained, and were used for strength and Young's modulus predictions, respectively.

Table 2.1 Information on composite materials prepared in this study

No	PHBH with 5.6 mol% of 3HH (vol%)	PHBH with 11.1 mol% of 3HH (vol%)	Glass Fiber (vol%)
1	100		0
2	95		5
3	90		10
4	84		16
5	77		23
6		100	0
7		95	5
8		90	10
9		84	16
10		77	23

Table 2.2 Properties of PHBH and glass fiber used for predictions

Material	Density (g/cm ³)	Young's modulus (GPa)	Strength (MPa)
PHBH5.6	1.20	1.43	-
PHBH11.1	1.19	0.76	-
Glass fiber	2.60	80.5	3450

2.2.4 Characterization of mechanical properties

Tensile tests were conducted to evaluate the mechanical properties of the composite materials. The tests were performed on the Type V specimen as per ASTM D638 standard, using Instron 5943 with a 1 kN load cell. Crosshead speed was 10 mm/min for all specimens. Five specimens were tested for each sample.

2.2.5 Characterization of thermal properties

Thermal properties of the composite materials were characterized using differential scanning calorimetry (DSC) (TA Q200). A DSC sample of 8 to 10 mg was prepared by cutting from the tensile specimen. The sample was heated from room temperature to 190°C at a rate of 10°C/min and kept at 190°C for 3 minutes to erase the thermal history. The sample was then cooled to -40°C at a rate of 5°C/min. Lastly, the sample was heated to 190°C at a rate of 10°C/min.

2.3 Result and Discussion

2.3.1 Fiber length frequency distribution and average fiber length

Figure 2.1 shows fiber length frequency distribution of selected representational injection-molded PHBH composite specimens with the least and greatest fiber amounts: PHBH5.6 with 5 vol% fiber (Figure 2.1a), PHBH5.6 with 23 vol% fiber (Figure 2.1b), PHBH11.1 with 5 vol% fiber (Figure 2.1c), and PHBH11.1 with 23 vol% fiber (Figure 2.1d). For both PHBH5.6 and PHBH11.1 composites, increase in fiber content was associated with the histogram shifting to the left (i.e., towards shorter fiber length).

The average length of fibers in the composite specimen as a function of volume fraction of fiber is shown in Figure 2.2. As volume fraction of fiber increased, average fiber length decreased significantly. This finding can be explained by fiber breakage occurring during compounding and injection molding, where greater fiber content leads to more fiber-fiber and fiber-equipment wall interactions. More such fiber interactions lead to more damage to fibers [23,24], leading to the fibers becoming shorter.

Figure 2.2 also shows that the average fiber length of PHBH5.6 was slightly longer than that of PHBH11.1 at a given fiber volume fraction. The relative difference in average fiber length is most likely due to PHBH11.1 having a relatively greater melt viscosity than PHBH5.6. The molecular weight of PHBH11.1 is greater than that of PHBH5.6 and, in general, polymers with higher molecular weight tend to have greater viscosity [25]. Greater melt viscosity led to shorter fiber lengths because greater melt viscosity results in

higher bending forces exerted on fibers during compounding and injection molding, leading to amplified damage of fibers [24].

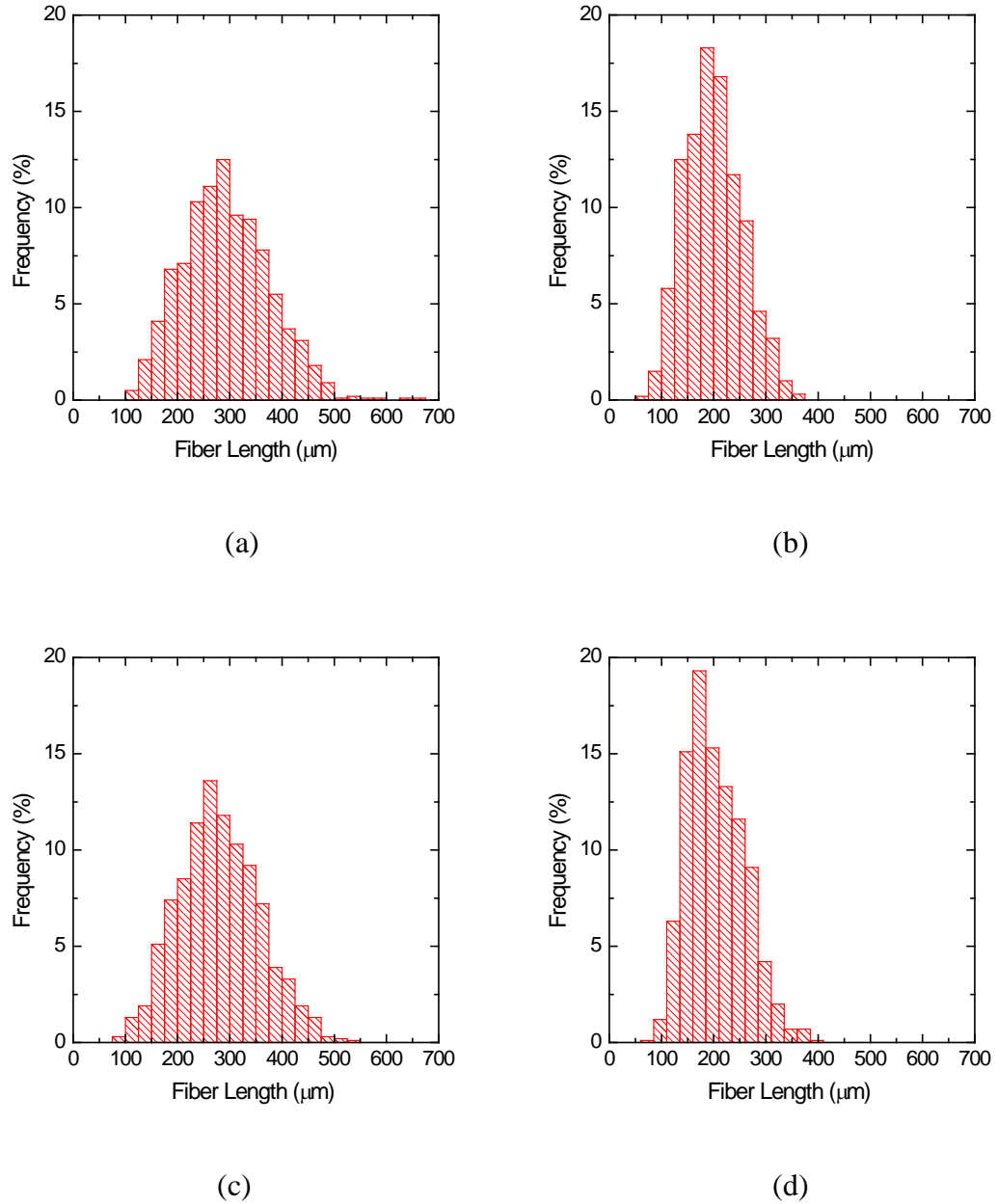


Figure 2.1 Fiber length frequency distribution for PHBH5.6 with (a) 5 vol% and (b)

23 vol% fibers as well as PHBH11.1 with (c) 5 vol% and (d) 23 vol% fibers

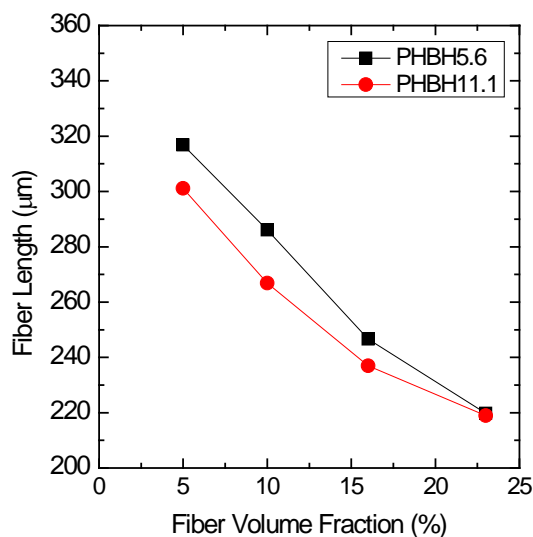


Figure 2.2 Average length of fibers in the injection-molded composite specimen versus the volume fraction of fiber

The supposed difference in melt viscosity between PHBH5.6 and PHBH11.1 is further supported by torque data. A torque value of a drive motor in an extruder during compounding can be related to melt viscosity of material, if temperature and rotational speed are constant. A lower torque can be the result of lower viscosity, due to its resulting lower resistance to rotation of screw shafts [26]. The torque of the drive motor in the mini-twin-screw extruder during the compounding of PHBH and glass fibers as a function of time is depicted in Figure 2.3. As expected, PHBH11.1 (Figure 2.3b) is found to have a greater torque and, therefore, greater viscosity than PHBH5.6 (Figure 2.3a). Additionally, Figure 2.3a and Figure 2.3b show that torque increased with increasing fiber content, supporting the aforementioned explanation of the finding of shorter fiber lengths with increasing fiber content.

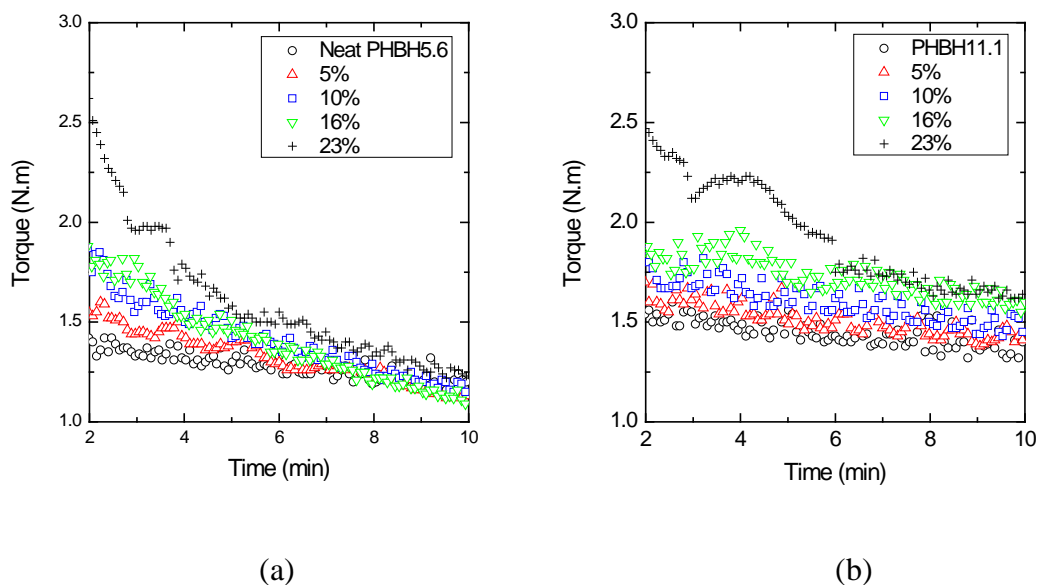


Figure 2.3 Torque versus time for (a) PHBH5.6 and (b) PHBH11.1 composites

2.3.2 Mechanical properties

Figure 2.4 illustrates typical stress–strain curves of PHBH5.6 composites (Figure 2.4) and PHBH11.1 composites (Figure 2.4) from tensile tests. The curves were obtained from PHBH with the following amounts (in vol%) of glass fiber: 0 (i.e. neat PHBH), 5, 10, 16, and 23. The neat specimens exhibited ductile failure while the glass fiber reinforced composites exhibited more brittle failure. Comparing the tensile test results of the two types of PHBH, the neat PHBH5.6 had higher strength but less ductility than PHBH11.1. This result agrees with those reported previously, in which PHBH gets softer and more flexible with the increase of 3HH content [12].

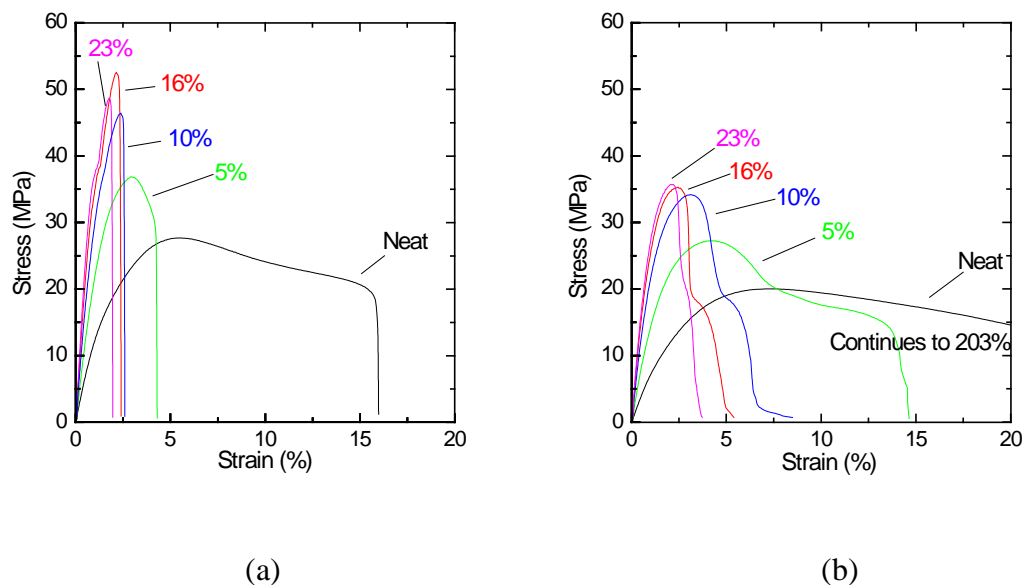


Figure 2.4 Stress-strain curves of (a) PHBH5.6 and (b) PHBH11.1 composites

Figure 2.5 summarizes the mechanical properties of the PHBH composites as a function of volume fraction of fiber. Young's modulus as a function of volume fraction of fiber is shown in Figure 2.5a. The Young's modulus of both PHBH5.6 and PHBH11.1 composites increased monotonically with increasing fiber content, with the Young's modulus of PHBH5.6 composites being higher than that of PHBH11.1 composites at a given fiber volume fraction. Figure 2.5b shows strength as a function of volume fraction of fiber. The strength of both PHBH5.6 and PHBH11.1 composites increased linearly up to 10 vol% of fiber, after which strength remained almost constant, despite further fiber content increase. This finding of lack of increase in strength at the greater fiber content could be explained by the decrease of fiber length, i.e., decrease of aspect ratio of fibers, at greater fiber content (as shown in Figure 2.2). Comparing the strength of the two PHBH types, similar to the trend found for Young's modulus, strength of PHBH5.6 composites was higher than that of PHBH11.1 counterparts at a given fiber volume

fraction. Figure 2.5c shows strain at failure as a function of volume fraction of fiber. Neat PHBH11.1 had a much greater failure strain than neat PHBH5.6. However, the addition of fiber decreased the failure strain of both PHBH5.6 and PHBH11.1 composites. Although PHBH11.1 composites exhibited a higher strain at failure than PHBH5.6 composites at a given fiber volume fraction, the difference was much smaller than that between the neat PHBH. Figure 2.5d shows fracture energy, which is defined as the area enclosed by the load-displacement curve, as a function of volume fraction of fiber. The trend is very similar to that observed in Figure 2.5c for strain at failure. This similarity suggests that, in the composite materials manufactured in this study, strain at failure contributed considerably to fracture energy.

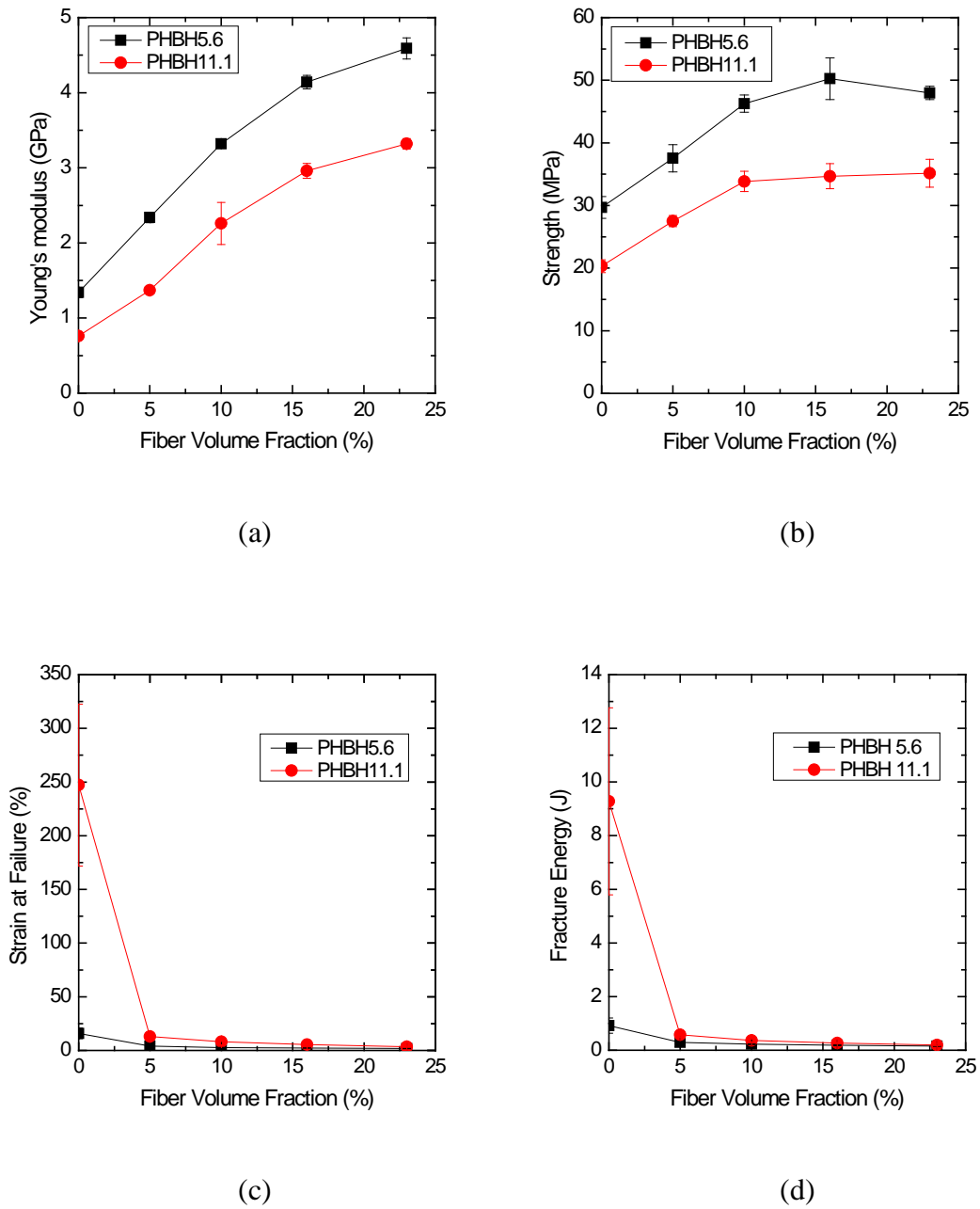


Figure 2.5 Mechanical properties of PHBH5.6 and PHBH11.1 composites: (a) Young's modulus, (b) Strength, (c) Strain at failure, and (d) Fracture energy

2.3.3 Prediction of Young's modulus

Young's modulus of glass fiber reinforced PHBH composites fabricated in this study was predicted by combining the Halpin-Tsai equations [27] and Tsai-Pagano equations [28].

Longitudinal and transverse Young's modulus of an aligned short-fiber composite material can be predicted using the Halpin-Tsai equations [27]. The equations for the longitudinal E_L and transverse Young's modulus E_T can be expressed as follows:

$$E_L = E_m \frac{1 + \xi \eta_L V_f}{1 - \eta_L V_f} \quad (2)$$

$$E_T = E_m \frac{1 + 2\eta_T V_f}{1 - \eta_T V_f} \quad (3)$$

where

$$\eta_L = \frac{(E_f/E_m) - 1}{(E_f/E_m) + \xi} \quad (4)$$

$$\eta_T = \frac{(E_f/E_m) - 1}{(E_f/E_m) + 2} \quad (5)$$

where E_m and E_f are the Young's modulus of matrix and fiber, respectively, V_f is the volume fraction of fibers, and ξ is the measure of the geometry of fiber. If a fiber is circular in cross-section, ξ may be calculated as follows:

$$\xi = 2(l/d) \quad (6)$$

where l and d are, respectively, length and diameter of a fiber.

Young's modulus E_{random} of a composite material with two-dimensional (in-plane) random fibers can be predicted using the following Tsai-Pagano equation [28]:

$$E_{random} = \frac{3}{8}E_L + \frac{5}{8}E_T \quad (7)$$

The Young's moduli of PHBH and glass fiber used for the Halpin-Tsai equations 4 and 5 are listed in Table 2.2. For equation 6, the average fiber length measured was used as a length of fiber.

Figure 2.6 illustrates predicted Young's modulus E_{random} of PHBH5.6 (Figure 2.6a) and PHBH11.1 (Figure 2.6b) composites as a function of volume fraction of fiber, together with the experimental values (see Figure 2.5a). The predictions agree well with the experimental results, the differences between them being less than 10% for both PHBH5.6 and PHBH11.1 composites at all the volume fractions of fibers, with the only exception being PHBH5.6 composites with 23 vol% fiber.

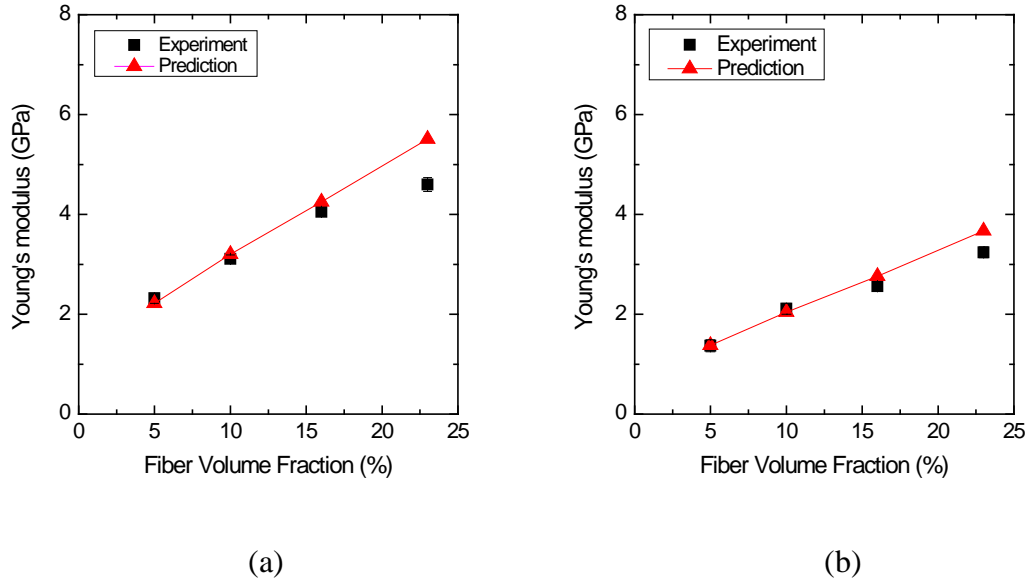


Figure 2.6 Young's modulus predicted by Halpin-Tsai and Tsai-Pagano equations for (a) PHBH5.6 and (b) PHBH11.1 composites

2.3.4 Prediction of strength

Ultimate tensile strength of glass fiber reinforced PHBH composites manufactured in this study was predicted using the Kelly-Tyson [29] and Bowyer-Bader models [30–33].

Strength of an aligned short-fiber composite material can be predicted using the Kelly-Tyson model [29] as follows:

$$\sigma_{uc} = \left(\frac{\tau L}{d}\right) V_f + \sigma_m(1 - V_f) \quad \text{for } L < L_c \quad (8)$$

$$\sigma_{uc} = \left(1 - \frac{L_c}{2L}\right) \sigma_f V_f + \sigma'_m(1 - V_f) \quad \text{for } L \geq L_c \quad (9)$$

where d is fiber diameter, τ is shear stress at the fiber-matrix interface, σ_f is fiber strength, σ_m is matrix strength, σ'_m is the stress carried by the matrix at the fiber failure strain, L is fiber length, and $L_c \left(= \frac{\sigma_f d}{2\tau} \right)$ is the critical fiber length, which is necessary for maximum stress in a fiber to reach the strength of fiber. The Kelly-Tyson model assumes that the matrix is rigid-plastic in shear, and that normal stress of fiber at the fiber ends is negligible and increases linearly towards the middle of the fiber, reaching a plateau when the distance from the ends is larger than $1/2L_c$.

If a composite material has fibers with different length [34,35] and/or orientation [35,36], the equations 8 and 9 can be modified, and tensile strength σ_{uc} of the composite material can be expressed as follows [35]:

$$\sigma_{uc} = \eta_0 \left\{ \sum_{L_i=L_{min}}^{L_i=L_c} \left(\frac{\tau L_i}{d} \right) V_i + \sum_{L_j=L_c}^{L_j=L_{max}} \left(1 - \frac{L_c}{2L_j} \right) \sigma_f V_j \right\} + \sigma'_m (1 - V_f) \quad (10)$$

where η_0 is the fiber orientation factor, d is fiber diameter, τ is the shear stress at the fiber-matrix interface, σ_f is fiber strength, σ'_m is the stress carried by the matrix at the fiber failure strain, L_i and L_j are the length of fibers having volume fractions V_i and V_j .

Bowyer and Bader [30–33] extended equation 10 to model a stress-strain curve of the composite material prior to failure. They proposed the critical fiber length L_e , which is strain dependent, expressed as follows:

$$L_e = \frac{E_f \epsilon_c d}{2\tau} \quad (11)$$

L_e is the fiber length necessary for maximum strain in a fiber to reach the matrix strain at a given composite strain ϵ_c . A stress-strain relationship of the composite material is expressed as follows:

$$\sigma_c = \eta_0 \left\{ \sum_{L_i=L_{min}}^{L_i=L_e} \frac{\tau L_i V_i}{d} + \sum_{L_j=L_e}^{L_j=L_{max}} E_f \epsilon_c \left(1 - \frac{E_f \epsilon_c d}{4L_j \tau} \right) V_j \right\} + \sigma'_m (1 - V_f) \quad (12)$$

This model can be simplified to $\sigma_c = \eta_0 \{X + Y\} + Z$, where X is the stress contribution from the subcritical fibers, Y is the stress contribution from the supercritical fibers, and Z is the stress contribution from the matrix. In the Bowyer-Bader model, the stress contribution from matrix was calculated from Young's modulus of the matrix and strain of the composite material. However, a stress-strain curve of many thermoplastics, including PHBH used in this study, is non-linear even at a low strain. Therefore, as suggested by Thomason [33], σ'_m was obtained directly from the stress-strain curve of neat PHBH at the strain of the composite material.

In order to predict tensile strength, σ_{uc} , of the composite material using equation 10, the parameters η_0 and τ need to be identified. In this study, the iterative method that Bowyer and Bader proposed [30,37] was used, which assumes that η_0 is independent of strain and constant for all fiber lengths, and that interfacial shear stress is independent of loading angle. The method is summarized as follows:

Step 1: The ratio R was determined using equation 13

$$R = \frac{\sigma_1 - Z_1}{\sigma_2 - Z_2} \quad (13)$$

where σ_1 and σ_2 are the tensile stress of the composite material, and Z_1 and Z_2 are the tensile stress of the matrix, at two selected strains, ε_1 and ε_2 . These stress values were obtained from the respective stress-strain curves.

Step 2: A value for τ was chosen arbitrarily and the critical fiber length at the strains ε_1 and ε_2 were calculated using equation 11. In this study, strains corresponding to 1/3 and 2/3 of the composite strength were selected as the strains ε_1 and ε_2 .

Step 3: The fiber contributions X_1 and Y_1 at the strain ε_1 as well as X_2 and Y_2 at the strain ε_2 were calculated. In this study, the volume fraction of fibers (V_i or V_j) with length L_i or L_j was calculated using fiber length frequency distribution data (see Figure 2.1). Ratio of fiber contribution R' was calculated using equation 14.

$$R' = \frac{X_1 + Y_1}{X_2 + Y_2} \quad (14)$$

Step 4: The previously assumed τ was adjusted until $R = R' \cdot \eta_0$ was then calculated by substituting the τ value into equation 12, and finally strength of the composite material was predicted using equation 10. Table 2.2 lists strength of fiber σ_f used in the equation 10.

Figure 2.7 demonstrates interfacial shear stress of PHBH5.6 and PHBH11.1 composites as a function of volume fraction of fiber. The figure shows that interfacial shear stress of

PHBH5.6 was slightly higher than that of PHBH11.1 at a given fiber volume fraction. Interfacial shear stress can be affected by various factors, such as residual stress due to differences between thermal expansion coefficients of matrix and fiber, chemical interaction between fiber and matrix, and friction between fiber and matrix [33]. As to be shown in the results of degree of crystallinity, PHBH5.6 composites had higher degree of crystallinity than PHBH11.1 composites, and the higher degree of crystallinity of PHBH5.6 composites may have caused greater matrix shrinkage during the solidification process, which thereby may have contributed to the higher interfacial shear stress. Nevertheless, further study is needed to test this speculation. The figure also shows that interfacial shear stress remained relatively constant with the change of fiber volume fraction.

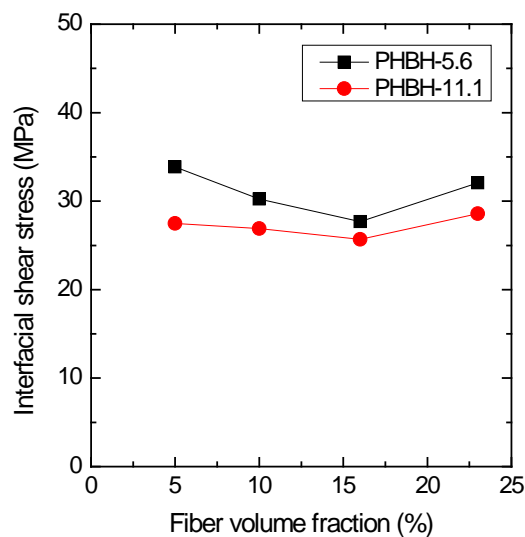


Figure 2.7 Interfacial shear stress of PHBH5.6 and PHBH11.1 composites

Figure 2.8 depicts fiber orientation factor of PHBH5.6 and PHBH11.1 composites as a function of volume fraction of fiber. Fiber orientation factors of both PHBH5.6 and PHBH11.1 composites decreased from approximately 0.3 to 0.2 with the increase of volume fraction of fiber. As can be seen from equations 10 and 12, the results suggest that the efficiency of fiber reinforcement decreased with fiber volume fraction. It is noted that the fiber orientation factor is an indirect fitting parameter obtained from a macroscopic stress-strain curve and is affected by other factors such as variation of strength of each fiber, imperfect interfacial bonding, and fiber end effects (i.e., normal stress at fiber ends), which are commonly found in short fiber composites [37].

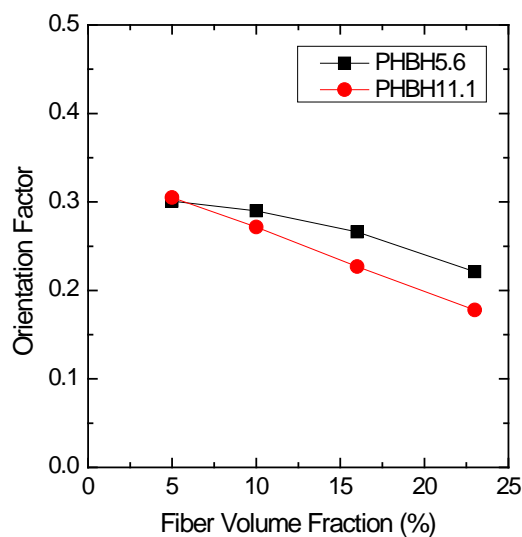


Figure 2.8 Fiber orientation factor of PHBH5.6 and PHBH11.1 composites

Figure 2.9 shows strength predicted by the Bowyer-Bader method for PHBH5.6 (Figure 2.9a) and PHBH11.1 (Figure 2.9b) composites as a function of volume fraction of fiber. The predicted values agree reasonably well with the experimental values for both

PHBH5.6 and PHBH11.1 composites. However, the difference between the predicted and experimental values was greatest at the greatest volume fraction of fiber (i.e., 23 vol%) for both PHBH5.6 and PHBH11.1 composites. One possible reason for the overestimation is that the strength of fiber used in the prediction was higher than that of fibers in the composite specimens. Thomason et al. demonstrated the wide range of fiber strength to be found in fibers used in glass mat thermoplastic (GMT). Differences in fiber strength were attributed to different levels of processing damage (from fiber–fiber contact and fiber-equipment wall contact) and fiber sizing protection efficiency [38]. Another possible reason for the overestimation is that voids at the interface and/or surface defects of fiber reduced the capability of stress transfer from the matrix to the fiber.

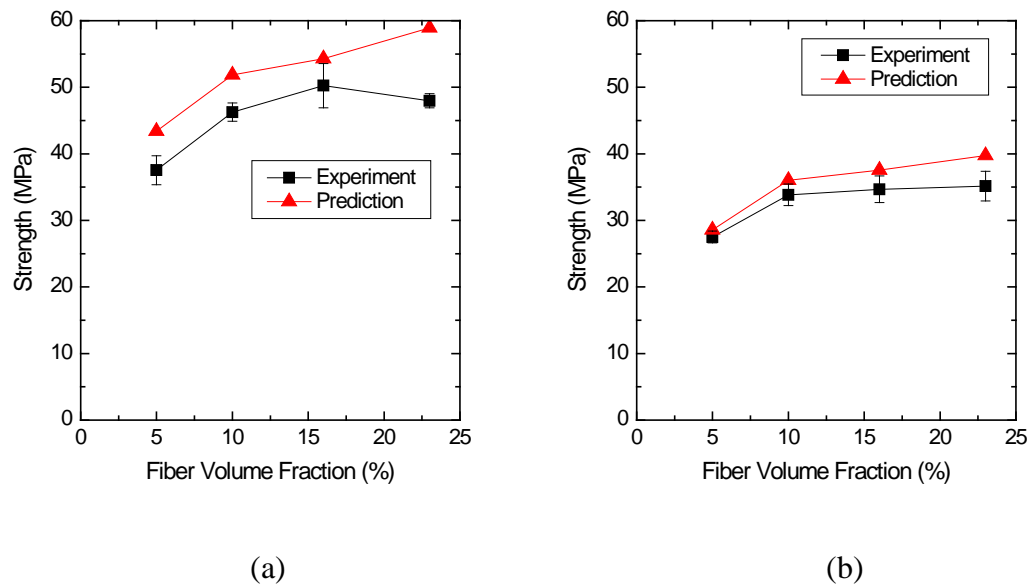


Figure 2.9 Strength predicted by the Bowyer-Bader method for (a) PHBH5.6 and (b) PHBH11.1 composites

2.3.5 Thermal properties

Figure 2.10 and Figure 2.11 depict the first and second DSC heating curves of PHBH5.6 and PHBH11.1 composites, respectively. In the first heating curve, PHBH5.6 composites (Figure 2.10a) showed two melting temperatures: T_{m1} and T_{m2} , where $T_{m1} < T_{m2}$. PHBH11.1 composites (Figure 2.10b), however, had one additional melting temperature T_a , which is lower than T_{m1} and T_{m2} (in the range between 45 to 52°C). The melting temperature T_a observed in PHBH11.1 composites originates from the melting of small imperfect crystallites that form during annealing at room temperature [39–41]. Since there is no annealing period at room temperature between the cooling and second heating scans, this annealing peak was not observed in the second heating curve (Figure 2.11a). The melting peak area at T_a was small and its contribution to the overall degree of crystallinity was insignificant. The melting temperature T_{m1} is related to the melting of crystals formed originally while the melting temperature T_{m2} is associated with the melting of crystals that were re-crystallized during the heating process [42,43].

Degree of crystallinity X_c of injection molded specimens was calculated from the first and second heating DSC curves and the following equation:

$$X_c = \frac{\Delta H_m - \Delta H_{cc}}{\Delta H_f(1 - W_f)} \times 100\% \quad (15)$$

where ΔH_m is enthalpy of fusion; ΔH_{cc} is enthalpy of cold crystallization; ΔH_f is enthalpy of fusion of fully crystalline PHB, which is taken to be 146 J/g [44]; and W_f is the weight fraction of fiber.

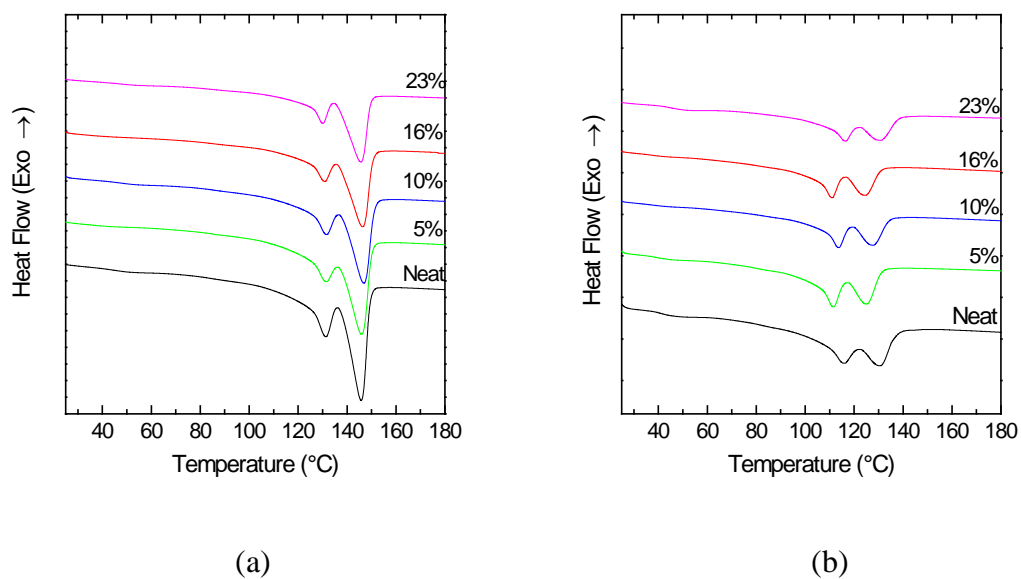


Figure 2.10 First DSC heating curves of (a) PHBH5.6 and (b) PHBH11.1 composites

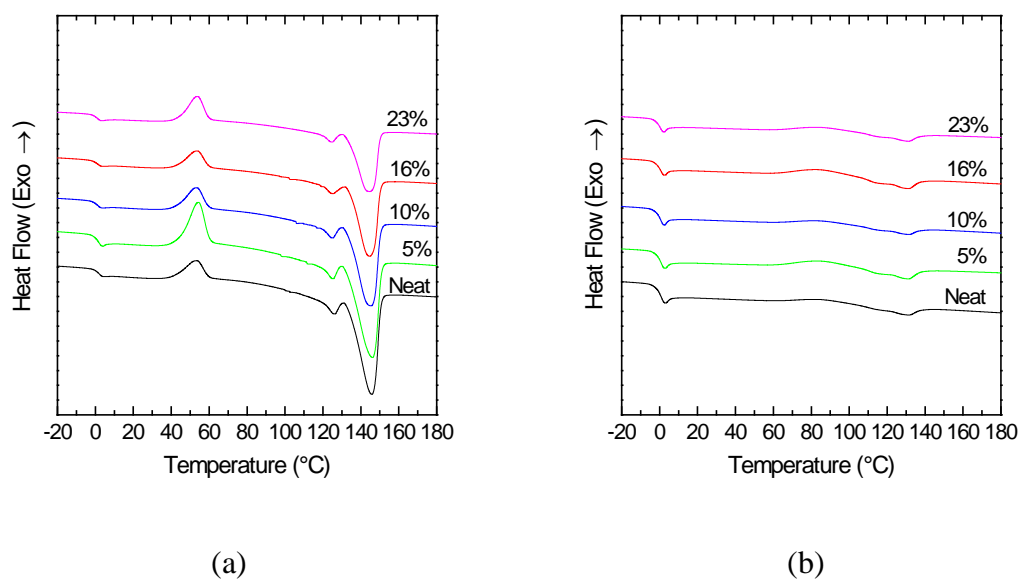


Figure 2.11 Second DSC heating curves of (a) PHBH5.6 and (b) PHBH11.1 composites

The thermal properties obtained from the first and second DSC heating curves are summarized in Table 2.3 and Table 2.4, respectively. The tables show that neat PHBH5.6 had higher melting temperatures T_{m1} and T_{m2} as well as degree of crystallinity X_c than neat PHBH11.1, which suggests that the secondary comonomer unit 3HH disturbed the poly(3-hydroxybutyrate)-type crystal lattice and suppressed crystallization [43]. It should be noted that the addition of glass fibers regardless of their content little affected degree of crystallinity of both PHBH5.6 and PHBH11.1. Additionally, for PHBH11.1 composites, the degree of crystallinity X_c obtained from the first heating curves (Figure 2.10b) was much higher than that obtained from the second heating curves (Figure 2.11b), which suggests that secondary crystallization occurred during solidification in injection molding and during the two days of annealing at room temperature. Furthermore, Table 2.4 shows that the addition of glass fibers, regardless of their content, little affected glass transition temperature T_g and cold crystallization temperature T_{cc} in both PHBH5.6 composites and PHBH11.1 composites.

Table 2.3 Thermal properties of PHBH5.6 and PHBH11.1 composites characterized from the first DSC curves

Sample	Fiber volume fraction (%)	T _a (°C)	ΔH _a (J/g)	T _{m1} (°C)	T _{m2} (°C)	ΔH _m ^{1st} (J/g)	X _c ^{1st} (%)
PHBH5.6	0	-	-	131.4	145.8	56.9	39.0
PHBH5.6	5	-	-	132.5	146.4	51.8	39.4
PHBH5.6	10	-	-	131.6	146.9	45.4	38.9
PHBH5.6	16	-	-	130.7	146.4	39.9	39.0
PHBH5.6	23	-	-	130.9	145.6	33.7	38.5
PHBH11.1	0	46.8	0.6	116.0	130.7	37.5	26.1
PHBH11.1	5	44.5	0.4	114.3	128.4	34.9	26.9
PHBH11.1	10	47.0	1.0	114.4	129.1	29.0	25.7
PHBH11.1	16	42.7	0.1	113.8	128.0	26.5	26.0
PHBH11.1	23	42.9	0.1	113.6	127.6	24.0	27.5

Table 2.4 Thermal properties of PHBH5.6 and PHBH11.1 composites characterized from the second DSC heating curves

Sample	Fiber volume fraction (%)	T _g (°C)	T _{cc} (°C)	T _{m1} (°C)	T _{m2} (°C)	ΔH _{cc} (J/g)	ΔH _m ^{2nd} (J/g)	X _c ^{2nd} (%)
PHBH5.6	0	1.5	53.8	126.1	145.8	8.6	54.4	31.4
PHBH5.6	5	1.4	54.4	125.3	146.2	18.3	56.7	29.2
PHBH5.6	10	0.9	53.6	125.0	145.4	10.2	46.1	30.8
PHBH5.6	16	0.7	53.9	125.3	144.6	8.3	40.4	31.3
PHBH5.6	23	0.5	54.0	124.9	144.6	10.4	36.6	30.0
PHBH11.1	0	0.0	81.5	113.6	131.5	3.4	5.0	1.1
PHBH11.1	5	-0.3	83.1	114.4	131.1	4.9	6.4	1.2
PHBH11.1	10	-0.2	81.4	113.1	131.5	2.7	3.9	1.0
PHBH11.1	16	-0.2	82.1	113.4	131.3	5.1	6.2	1.1
PHBH11.1	23	-0.6	82.4	115.7	131.1	3.4	4.5	1.2

Figure 2.12 illustrates DSC cooling curves of PHBH5.6 (Figure 2.12a) and PHBH11.1 (Figure 2.12b) composites. PHBH5.6 composites showed crystallization temperature around 50°C, but PHBH11.1 composites did not, which indicates that the crystallization

rate decreased with the increase of 3HH content and that there was not enough time for crystals to form in PHBH11.1 composites during the cooling process. It is noted that another peak was observed next to the crystallization peak in PHBH5.6 composites with 16 and 23 vol% of fiber. Further study is needed to investigate this peak.

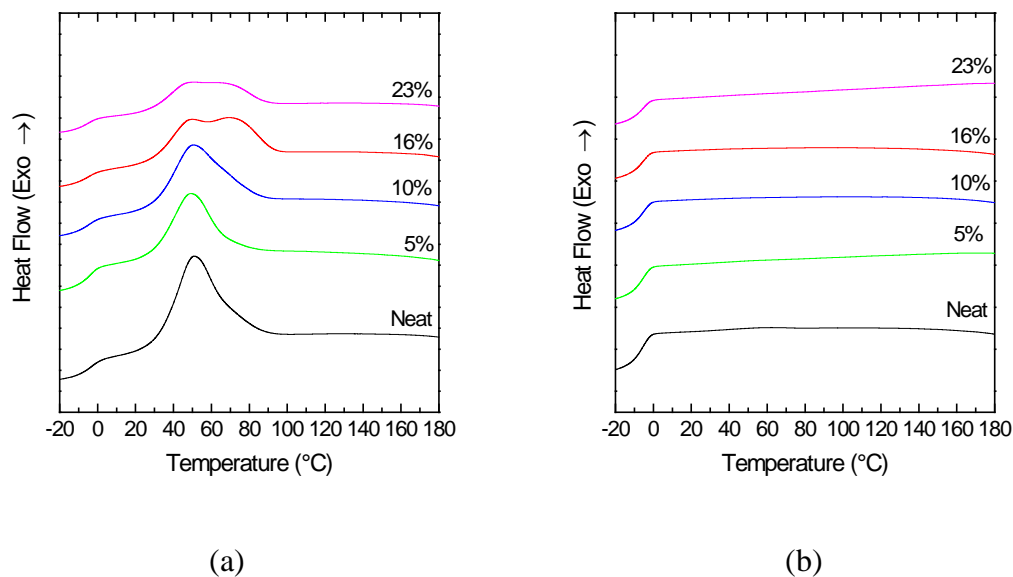


Figure 2.12 DSC cooling curves of (a) PHBH5.6 and (b) PHBH11.1 composites

2.3.6 Non-isothermal crystallization kinetics

Since crystallization temperature was not observed in PHBH11.1, crystallization kinetics of only PHBH5.6 composites were analyzed. The relative degree of crystallinity as a function of temperature can be calculated using the DSC cooling curves and the following equation [45]:

$$X(T) = \frac{\int_{T_0}^T \left(\frac{dH_c}{dT}\right) dT}{\int_{T_0}^{T_\infty} \left(\frac{dH_c}{dT}\right) dT} \quad (16)$$

where T_0 and T_∞ represent onset and end-crystallization temperatures, respectively.

Crystallization kinetics under isothermal conditions are often analyzed using the following Avrami equation [46]:

$$X(t) = 1 - \exp(-z_t t^n) \quad (17)$$

where $X(t)$ is the relative degree of crystallinity, n is the Avrami exponent that depends on the nature of the nucleation mechanism and growth geometry of crystals, z_t is the crystallization rate constant that involves both nucleation and growth rate parameters, and t is the time.

In non-isothermal crystallization processes, the relationship between crystallization time t and temperature T is given by:

$$t = \frac{|T_0 - T|}{\phi} \quad (18)$$

By taking into account the time-temperature relationship of equation 18, equation 17 can be transformed into the double-logarithmic form,

$$\log[-\ln(1 - X(T))] = \log Z_t + n \log t \quad (19)$$

The parameters n (slope) and Z_t (intercept) were determined by plotting $\log[-\ln(1 - X(T))]$ against $\log t$.

Jeziorny [47] pointed out that the composite rate constant z_t should be adequately corrected to take into account the cooling rate of the polymer. Assuming constant cooling rate ϕ , the parameter characterizing kinetics of non-isothermal crystallization was given as follows:

$$\log Z_c = \frac{\log Z_t}{\phi} \quad (20)$$

The crystallization half-time $t_{1/2}$, which is defined as the time taken from the onset of the crystallization until 50% completion, was calculated as follows:

$$t_{1/2} = \left(\frac{\ln 2}{Z_c} \right)^{\frac{1}{n}} \quad (21)$$

Figure 2.13 shows Avrami plots, i.e., plots of $\log[-\ln(1 - X(T))]$ versus $\log t$, of PHBH5.6 composites. All of the composites showed a linear line and there was no significant shift of the lines. Kinetic parameters determined by the Avrami equation with Jeziorny's correction are summarized in Table 2.5. The Avrami constant n did not change until the fiber volume fraction of 10%, but decreased with the further addition of glass fiber (16 and 23 vol%). The decrease of n value indicates the change in the nucleation mechanism and growth geometry of crystals, which may be related to the appearance of two crystallization peaks in the DSC cooling curves for PHBH5.6 with 16 and 23 vol% fiber (Figure 2.12). Furthermore, the addition of glass fiber did not affect the z_c values and crystallization half-time of PHBH5.6 regardless of the amount of fiber added.

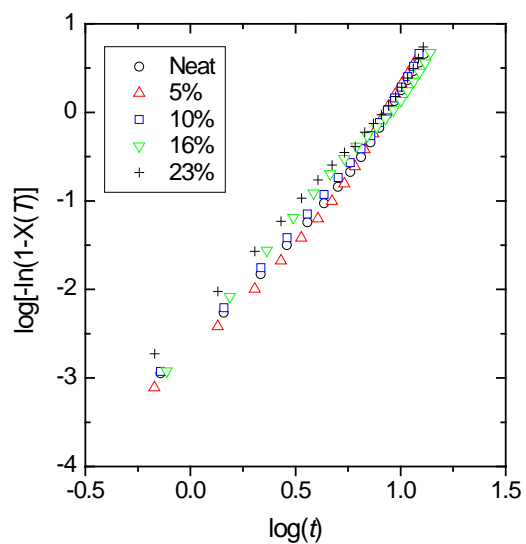


Figure 2.13 Avrami plots of PHBH5.6 composites

Table 2.5 Thermal properties of PHBH5.6 composites characterized from the DSC cooling curves and non-isothermal kinetic parameters calculated from the modified Avrami equation

Sample	Fiber volume fraction (%)	T_0 (°C)	T_c (°C)	ΔH_c (J/g)	Z_c	n	$t_{1/2}$ (min)
PHBH5.6	0	92.2	51.0	33.1	0.28	2.95	1.36
PHBH5.6	5	88.5	49.2	22.2	0.26	3.09	1.37
PHBH5.6	10	91.4	50.0	26.4	0.29	2.92	1.35
PHBH5.6	16	94.0	49.1, 69.4	26.1	0.31	2.66	1.35
PHBH5.6	23	92.5	48.6, 66.6	15.2	0.30	2.65	1.38

2.4 Conclusion

The effects of glass fiber on the mechanical and thermal properties of PHBH with 3HH molar contents of 5.6% and 11.1% were investigated. PHBH composite specimens were successfully manufactured through melt-compounding and injection molding processes. Tensile test results suggested that the addition of glass fiber significantly improved the Young's modulus and strength of both PHBH5.6 and PHBH11.1. Young's modulus increased monotonically, in a linear fashion, with increasing fiber content until 10 vol% fiber loading, after which strength stopped improving. Young's modulus of PHBH composites was compared with values predicted from the Halpin-Tsai and Tsai-Pagano equations while strength of PHBH composites was predicted using numbers from the modified Kelly-Tyson model with the Bowyer-Bader method. Both predictions agreed reasonably well with experimental values. DSC results suggested that the addition of glass fiber had little effect on the degree of crystallinity of PHBH5.6 and PHBH11.1. Furthermore, analysis of non-isothermal crystallization kinetics of PHBH5.6, using the modified Avrami equation, showed that the addition of glass fiber had little effect on the crystallization half-time.

2.5 Reference

- [1] Yu L. *Biodegradable Polymer Blends and Composites from Renewable Resources*. Wiley; 2008.
- [2] Philip S, Keshavarz T, Roy I. Polyhydroxyalkanoates: biodegradable polymers with a range of applications. *J Chem Technol Biotechnol* 2007;82:233–47.

- [3] Chen G-Q. A microbial polyhydroxyalkanoates (PHA) based bio- and materials industry. *Chem Soc Rev* 2009;38:2434–46.
- [4] Williams SF, Martin DP, Horowitz DM, Peoples OP. PHA applications: addressing the price performance issue. *Int J Biol Macromol* 1999;25:111–21.
- [5] Chen G-Q, Wu Q. The application of polyhydroxyalkanoates as tissue engineering materials. *Biomaterials* 2005;26:6565–78.
- [6] Sudesh K, Abe H, Doi Y. Synthesis, structure and properties of polyhydroxyalkanoates: biological polyesters. *Prog Polym Sci* 2000;25:1503–55.
- [7] Laycock B, Halley P, Pratt S, Werker A, Lant P. The chemomechanical properties of microbial polyhydroxyalkanoates. *Prog Polym Sci* 2013;38:536–83.
- [8] Steinbüchel A, Valentin HE. Diversity of bacterial polyhydroxyalkanoic acids. *FEMS Microbiol Lett* 1995;128:219–28.
- [9] Lee SY. Bacterial polyhydroxyalkanoates. *Biotechnol Bioeng* 1996;49:1–14.
- [10] Madison LL, Huisman GW. Metabolic Engineering of Poly(3-Hydroxyalkanoates): From DNA to Plastic. *Microbiol Mol Biol Rev* 1999;63:21–53.
- [11] Noda I, Green PR, Satkowski MM, Schechtman LA. Preparation and properties of a novel class of polyhydroxyalkanoate copolymers. *Biomacromolecules* 2005;6:580–6.

- [12] Doi Y, Kitamura S, Abe H. Microbial Synthesis and Characterization of Poly(3-hydroxybutyrate-co-3-hydroxyhexanoate). *Macromolecules* 1995;28:4822–8.
- [13] Alata H, Aoyama T, Inoue Y. Effect of Aging on the Mechanical Properties of Poly(3-hydroxybutyrate-co-3-hydroxyhexanoate). *Macromolecules* 2007;40:4546–51.
- [14] Asrar J, Valentin HE, Berger PA, Tran M, Padgett SR, Garbow JR. Biosynthesis and properties of poly(3-hydroxybutyrate-co-3-hydroxyhexanoate) polymers. *Biomacromolecules* 2002;3:1006–12.
- [15] Gibson RF. *Principles of Composite Material Mechanics*, Third Edition. CRC Press; 2011.
- [16] Huda MS, Drzal LT, Misra M, Mohanty AK. Chopped glass and recycled newspaper as reinforcement fibers in injection molded poly(lactic acid) (PLA) composites: A comparative study. *Compos Sci Technol* 2006;66:1813–24.
- [17] Laura D. Effect of glass fiber surface chemistry on the mechanical properties of glass fiber reinforced, rubber-toughened nylon 6. *Polymer (Guildf)* 2002;43:4673–87.
- [18] Yu Z, Yang Y, Zhang L, Ding Y, Chen X, Xu K. Study on short glass fiber-reinforced poly(3-hydroxybutyrate-co-4-hydroxybutyrate) composites. *J Appl Polym Sci* 2012;126:822–9.

- [19] Hosoda N, Tsujimoto T, Uyama H. Green Composite of Poly(3-hydroxybutyrate-co-3-hydroxyhexanoate) Reinforced with Porous Cellulose. *ACS Sustain Chem Eng* 2014;2:248–53.
- [20] Josefine Fischer J, Aoyagi Y, Enoki M, Doi Y, Iwata T. Mechanical properties and enzymatic degradation of poly([R]-3-hydroxybutyrate-co-[R]-3-hydroxyhexanoate) uniaxially cold-drawn films. *Polym Degrad Stab* 2004;83:453–60.
- [21] Lim J, Chong MSK, Teo EY, Chen G-Q, Chan JKY, Teoh S-H. Biocompatibility studies and characterization of poly(3-hydroxybutyrate-co-3-hydroxyhexanoate)/polycaprolactone blends. *J Biomed Mater Res B Appl Biomater* 2013;101:752–61.
- [22] Hassan MK, Abou-Hussein R, Zhang X, Mark JE, Noda I. Biodegradable Copolymers of 3-Hydroxybutyrate-co-3-Hydroxyhexanoate (Nodax™), Including Recent Improvements in their Mechanical Properties. *Mol Cryst Liq Cryst* 2006;447:23/[341] – 44/[362].
- [23] Fu S-Y, Lauke B, Mäder E, Yue C-Y, Hu X. Tensile properties of short-glass-fiber- and short-carbon-fiber-reinforced polypropylene composites. *Compos Part A Appl Sci Manuf* 2000;31:1117–25.
- [24] Thomason JL. Micromechanical parameters from macromechanical measurements on glass reinforced polypropylene. *Compos Sci Technol* 2002;62:1455–68.

- [25] Carrasco F, Pagès P, Gámez-Pérez J, Santana OO, MasPOCH ML. Processing of poly(lactic acid): Characterization of chemical structure, thermal stability and mechanical properties. *Polym Degrad Stab* 2010;95:116–25.
- [26] Fan* RR, Zhou* LX, Li DX, Zhang DM, Wu M, Guo G. Preparation and Characterization of Composites Based on Poly (Butylene Succinate) and Poly (Lactic Acid) Grafted Tetracalcium Phosphate. *J Macromol Sci Part B* 2013;53:296–308.
- [27] Affdl JCH, Kardos JL. The Halpin-Tsai equations: A review. *Polym Eng Sci* 1976;16:344–52.
- [28] Tsai S, Pagano N. Invariant properties of composite materials. 1968.
- [29] Kelly A, Tyson WR. Tensile properties of fibre-reinforced metals: Copper/tungsten and copper/molybdenum. *J Mech Phys Solids* 1965;13:329–50.
- [30] Bowyer WH, Bader MG. On the re-inforcement of thermoplastics by imperfectly aligned discontinuous fibres. *J Mater Sci* 1972;7:1315–21.
- [31] Bader MG, Bowyer WH. The mechanical properties of thermoplastics strengthened by short discontinuous fibres. *J Phys D Appl Phys* 1972;5:2215–25.
- [32] Bader MG, Bowyer WH. An improved method of production for high strength fibre-reinforced thermoplastics. *Composites* 1973;4:150–6.
- [33] Thomason J. Interfacial strength in thermoplastic composites - at last an industry friendly measurement method? *Compos Part A Appl Sci Manuf* 2002;33:1283–8.

- [34] Yu Z. Prediction of mechanical properties of short kevlar fiber-nylon-6,6 composites. *Polym Compos* 1994;15:64.
- [35] Fu S. Effects of fiber length and fiber orientation distributions on the tensile strength of short-fiber-reinforced polymers. *Compos Sci Technol* 1996;56:1179–90.
- [36] Bernasconi A, Rossin D, Armani C. Analysis of the effect of mechanical recycling upon tensile strength of a short glass fibre reinforced polyamide 6,6. *Eng Fract Mech* 2007;74:627–41.
- [37] Beckermann GW, Pickering KL. Engineering and evaluation of hemp fibre reinforced polypropylene composites: Micro-mechanics and strength prediction modelling. *Compos Part A Appl Sci Manuf* 2009;40:210–7.
- [38] Thomason JL, Vlug MA, Schipper G, Krikor HGLT. Influence of fibre length and concentration on the properties of glass fibre-reinforced polypropylene: Part 3. Strength and strain at failure. *Compos Part A Appl Sci Manuf* 1996;27:1075–84.
- [39] Pan P, Liang Z, Nakamura N, Miyagawa T, Inoue Y. Uracil as nucleating agent for bacterial poly[(3-hydroxybutyrate)-co-(3-hydroxyhexanoate)] copolymers. *Macromol Biosci* 2009;9:585–95.
- [40] Ye H-M, Wang Z, Wang H-H, Chen G-Q, Xu J. Different thermal behaviors of microbial polyesters poly(3-hydroxybutyrate-co-3-hydroxyvalerate-co-3-hydroxyhexanoate) and poly(3-hydroxybutyrate-co-3-hydroxyhexanoate). *Polymer (Guildf)* 2010;51:6037–46.

- [41] Hu Y, Zhang J, Sato H, Noda I, Ozaki Y. Multiple melting behavior of poly(3-hydroxybutyrate-co-3-hydroxyhexanoate) investigated by differential scanning calorimetry and infrared spectroscopy. *Polymer (Guildf)* 2007;48:4777–85.
- [42] Guo C, Zhou L, Lv J. Effects of expandable graphite and modified ammonium polyphosphate on the flame-retardant and mechanical properties of wood flour-polypropylene composites. *Polym Polym Compos* 2013;21:449–56.
- [43] Watanabe T, He Y, Fukuchi T, Inoue Y. Comonomer Compositional Distribution and Thermal Characteristics of Bacterially Synthesized Poly(3-hydroxybutyrate-co-3-hydroxyhexanoate)s. *Macromol Biosci* 2001;1:75–83.
- [44] Barham PJ, Keller A, Otun EL, Holmes PA. Crystallization and morphology of a bacterial thermoplastic: poly-3-hydroxybutyrate. *J Mater Sci* 1984;19:2781–94.
- [45] Bianchi O, Oliveira RVB, Fiorio R, Martins JDN, Zattera AJ, Canto LB. Assessment of Avrami, Ozawa and Avrami–Ozawa equations for determination of EVA crosslinking kinetics from DSC measurements. *Polym Test* 2008;27:722–9.
- [46] Avrami M. Kinetics of phase change. I: General theory. *J Chem Phys* 1939;7:1103–12.
- [47] Jeziorny A. Parameters characterizing the kinetics of the non-isothermal crystallization of poly(ethylene terephthalate) determined by d.s.c. *Polymer (Guildf)* 1978;19:1142–4.

Chapter 3

3 Effects of Thermoplastic Elastomers on Mechanical and Thermal Properties of Glass Fiber Reinforced Poly(3-hydroxybutyrate-co-3-hydroxyhexanoate)

3.1 Introduction

Poly(hydroxyalkanoates) (PHAs) are biodegradable and biocompatible plastics, and are commonly used in the packaging [1,2] and medical fields [1,2] (especially in tissue engineering [3,4]). PHAs are also known as environmentally friendly bioplastics because their production, which uses microorganisms, has relatively low CO₂ emission and is independent from petroleum sources [5–7]. Poly(3-hydroxybutyrate) (PHB) is a homopolymer and is one of the most well-studied PHAs. However, due to its high degree of crystallinity, PHB is brittle [5,6,8], which limits its industrial applications. To modify the physical properties of PHB, different types of comonomers have been introduced into PHB to form a copolymer [9,10].

Poly(3-hydroxybutyrate-co-3-hydroxyhexanoate) (PHBH) is one of the copolymers of PHB. The addition of the 3-hydroxyhexanoate (3HH) unit broadens process temperature as well as increases ductility, but decreases modulus and strength [11–13]. In our recent study [14], we demonstrated that the addition of glass fibers is an effective method for improving both Young's modulus and tensile strength of PHBH. However, the addition of glass fibers reduced ductility and energy absorbed in fracture of PHBH.

One way to improve ductility and/or energy absorbed in fracture of glass fiber reinforced composite materials is addition of thermoplastic elastomers. Various thermoplastic elastomers have been added to glass fiber reinforced composite materials [15–26]. Although incorporation of a thermoplastic elastomer decreases strength and modulus [25,27], it is possible to achieve a balance in strength, modulus, and toughness of glass fiber reinforced polymer composites. Toughening mechanisms of plastic/thermoplastic elastomer blends are associated with plastic deformation, such as crazing and/or shear yielding, around thermoplastic elastomer particles. On the other hand, toughening mechanisms of glass fiber/plastic composites include crack deflection by fiber, fiber/matrix debonding, fiber bridging of cracks, and fiber pull-out [26]. In general, the toughening mechanisms of glass fiber/plastic/thermoplastic elastomer hybrid composites involve a combination of these energy absorption mechanisms.

Styrene-ethylene-butadiene-styrene (SEBS) and maleic anhydride grafted styrene-ethylene-butadiene-styrene (SEBS-MA) are two thermoplastic elastomers that have been applied to glass fiber reinforced polypropylene (PP) [15–17] and nylon [21–24]. Tjong et al. [16] reported that the addition of SEBS and SEBS-MA increased notched Izod impact strength of glass fiber reinforced PP. Also, they found that SEBS promoted the crystallization of PP by acting as active nucleation sites, but SEBS-MA retarded the crystallization of PP. Similarly, Karayannidis et al. [21] reported that the addition of SEBS-MA increased notched Izod impact strength of glass fiber reinforced nylon-6,6. Additionally, they found that nylon-6,6 and SEBS-MA are immiscible and that SEBS-MA slightly decreased the degree of crystallinity of nylon-6,6.

In this study, these two types of thermoplastic elastomers, SEBS and SEBS-MA, were added to improve ductility and energy absorbed in fracture of glass fiber reinforced PHBH composites. To the authors' knowledge, this is the first study to report on toughening of glass fiber reinforced PHBH composites using thermoplastic elastomers. Since SEBS and SEBS-MA are immiscible with PHBH, as shown in the results from differential scanning calorimetry (DSC), it is expected that PHBH/glass fiber/thermoplastic elastomer composites will have one of the following morphologies: (a) glass fibers and rubber particles separately dispersed in the PHBH matrix, (b) fibers encapsulated by rubber, or (c) a mixture of (a) and (b). This study discusses the relationships between the morphology and mechanical properties, and also investigates the effects of SEBS and SEBS-MA on thermal properties, including crystallization kinetics, of glass fiber reinforced PHBH composites.

3.2 Experimental

3.2.1 Materials

This study used two types of PHBH, supplied by Kaneka Corporation. One type (hereafter referred to as PHBH5.6) contained 5.6 mol% 3HH and had a weight-average molecular weight of 555,000 g/mol. The other type (hereafter referred to as PHBH11.1) contained 11.1 mol% 3HH and had a weight-average molecular weight of 622,000 g/mol. The glass fibers (GF) used were chopped strand glass fibers (OCW-272, supplied by Owens Corning), with a diameter of 10 μm and a length ranging from 4 to 4.5 mm. Two types of thermoplastic elastomer (TE) were employed in this study. The first one (hereafter referred to as SEBS) was a SEBS copolymer (G1652M, Kraton Polymers) with

a polystyrene content of 30 wt%. The other (hereafter referred to as SEBS-MA) was maleated SEBS copolymer (FG1901X, Kraton Polymers) with a polystyrene content of 30 wt%.

3.2.2 Fabrication of composites

PHBH was dried at 80°C using a convection oven to eliminate possible moisture. Composite samples were prepared using a mini-twin-screw extruder (HAAKE MiniLab). PHBH, GF, and TE were compounded with conical co-rotating screws at 100 rpm for 10 minutes. The degree of fill in the extruder was set to 100% and barrel temperature was set to 150°C. The resulting molten composite was transferred to a preheated mini-injection molding machine (HAAKE MiniJet), which then injected the melt into a mold with a 240 bar injection pressure. Injection cylinder and mold temperatures were set to 150°C and 70°C, respectively. In this study, six types of composite material were prepared. Information on the composite materials is summarized in Table 3.1. GF and TE contents were set to 20 wt% and 30 wt%, respectively.

3.2.3 Measurement of fiber length

To measure length of glass fibers in an injection-molded specimen, PHBH and TE in the composite specimen were burnt off in a convection oven at 600°C for 30 minutes. The leftover ash and fibers were dispersed in water to extract fibers. A few drops of fiber-water were then cast onto a glass slide. Fiber length was measured using an optical microscope (Laborlux 11 POL) equipped with a digital camera, and imaging analysis software (Infinity Analyze). Lengths of about 1000 fibers were measured for each

specimen. Based on the resulting data, fiber length frequency distribution and weighted average fiber length were obtained.

Table 3.1 Information on composite materials prepared in this study

Name	PHBH with 5.6 mol% of 3HH (wt%)	PHBH with 11.1 mol% of 3HH (wt%)	Glass Fiber (wt%)	SEBS (wt%)	SEBS-MA (wt%)
PHBH5.6/GF	100		0	0	0
PHBH5.6/GF/SEBS	50		20	30	0
PHBH5.6/GF/SEBS-MA	50		20	0	30
PHBH11.1/GF		100	0	0	0
PHBH11.1/GF/SEBS		50	20	30	0
PHBH11.1//GF/SEBS-MA		50	20	0	30

3.2.4 Characterization of mechanical properties

Tensile and notched Izod impact tests were conducted to evaluate the mechanical properties of the composite materials. The tensile tests were performed on the Type V specimen as per ASTM D638 standard, using Instron 5943 with a 1 kN load cell. Crosshead speed was 10 mm/min for all specimens. Notched Izod impact tests, based on the ASTM D256 procedure, were executed using a conventional pendulum-type Izod impact tester (92T, Tinius Olsen). The specimens on the face of the notch (Test Method

A in the ASTM D256) were impacted by the striker. At least five specimens were used in each of the mechanical tests.

3.2.5 Observation of fracture surface

Fracture surface was observed by scanning electron microscopy (SEM). The fracture surface of tensile and notched Izod impact specimens was coated with a thin layer of osmium using an osmium plasma coater (OPC80T, Filgen) and then examined using a scanning electron microscope (LEO 1540XB, Zeiss).

3.2.6 Characterization of thermal properties

Thermal properties of the composite materials were characterized by DSC, using a TA Q200 differential scanning calorimeter. A DSC sample of 8 to 10 mg was prepared by cutting from the tensile specimen. The sample was heated from room temperature to 190°C at a rate of 10°C/min and kept at 190°C for 3 minutes to erase the thermal history. The sample was then cooled to -40°C at a rate of 5°C/min. Lastly, the sample was heated to 190°C at a rate of 10°C/min.

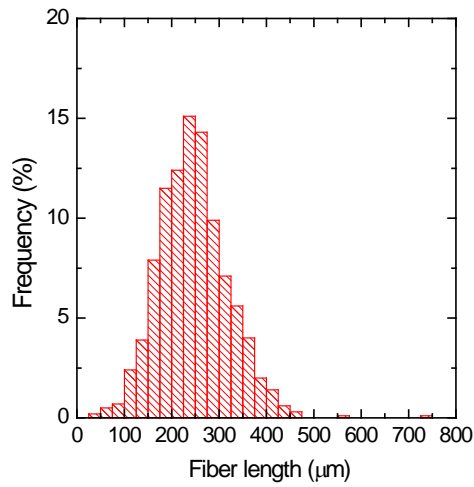
3.3 Results and Discussion

3.3.1 Fiber length frequency distribution and average fiber length

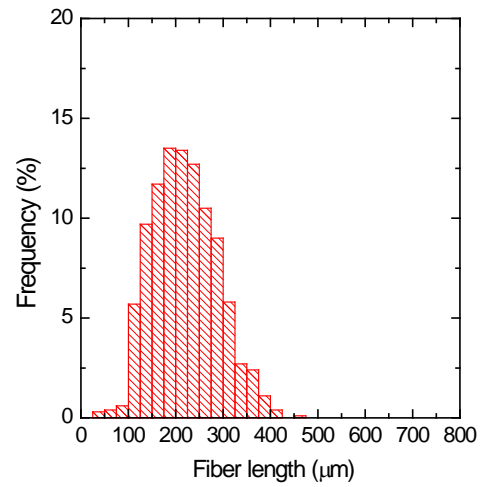
Figure 3.1 and Figure 3.2 show fiber length frequency distribution of representational injection-molded PHBH5.6/GF and PHBH11.1/GF composites, respectively, in three conditions: PHBH/GF without thermoplastic elastomers (Figure 3.1a and Figure 3.2a), with SEBS (Figure 3.1b and Figure 3.2b), and with SEBS-MA (Figure 3.1c and Figure

3.2c). For both PHBH5.6 and PHBH11.1 composites, the addition of SEBS or SEBS-MA was associated with the histogram shifting slightly to the left (i.e., towards shorter fiber length), and with a slight decrease in average fiber length in the composite specimens, as summarized in Figure 3.3.

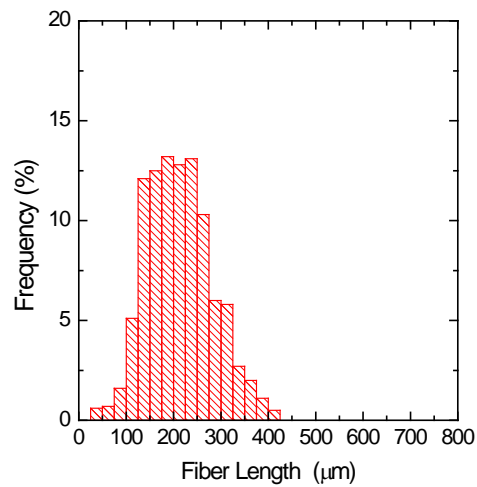
Figure 3.4 depicts the torque of the drive motor in the mini-twin-screw extruder during the compounding of PHBH, GF, and TE (i.e., SEBS or SEBS-MA) as a function of time. A torque value of a drive motor in an extruder during compounding can be related to melt viscosity of the material being compounded, if temperature and rotational speed are constant. A lower torque can be the result of lower viscosity, due to its resulting lower resistance to rotation of screw shafts [28]. The addition of SEBS and SEBS-MA increased torque, and therefore presumably viscosity as well, of both PHBH5.6/GF (Figure 3.4a) and PHBH11.1/GF (Figure 3.4b). Greater melt viscosity led to shorter fiber lengths because greater melt viscosity results in higher bending forces exerted on fibers during compounding and injection molding, leading to amplified damage of fibers [29].



(a)

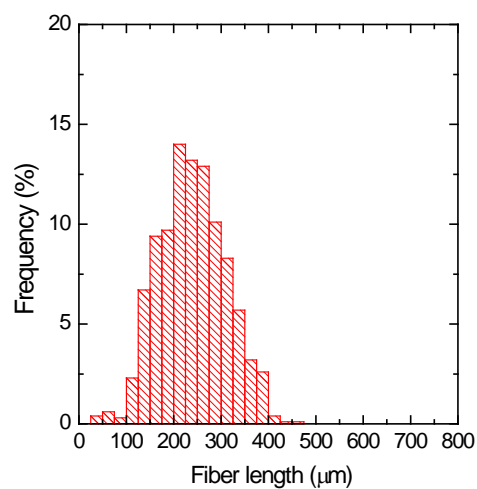


(b)

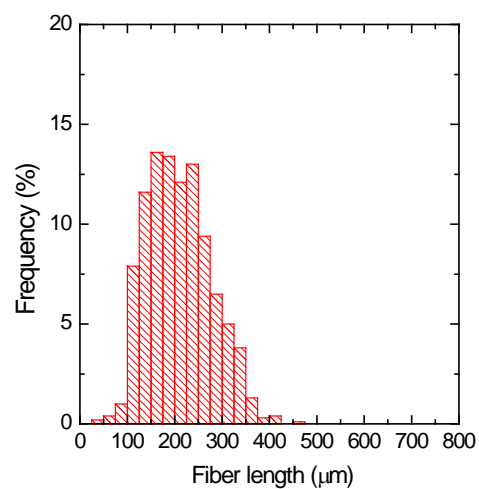


(c)

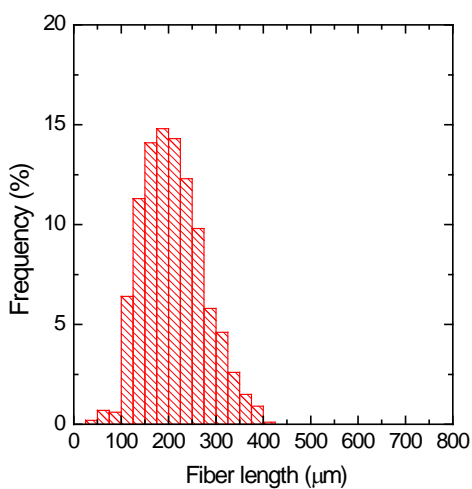
Figure 3.1 Fiber length frequency distribution for PHBH5.6/GF composites with (a) no thermoplastic elastomers, (b) SEBS, and (c) SEBS-MA



(a)



(b)



(c)

Figure 3.2 Fiber length frequency distribution for PHBH11.1/GF composites with (a) no thermoplastic elastomers, (b) SEBS, and (c) SEBS-MA

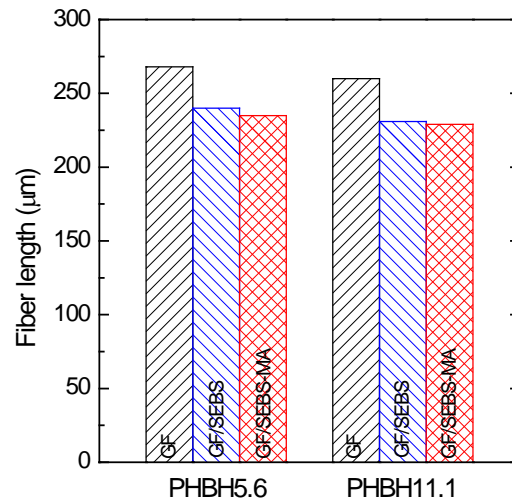


Figure 3.3 Average length of fibers in the injection-molded composite specimens

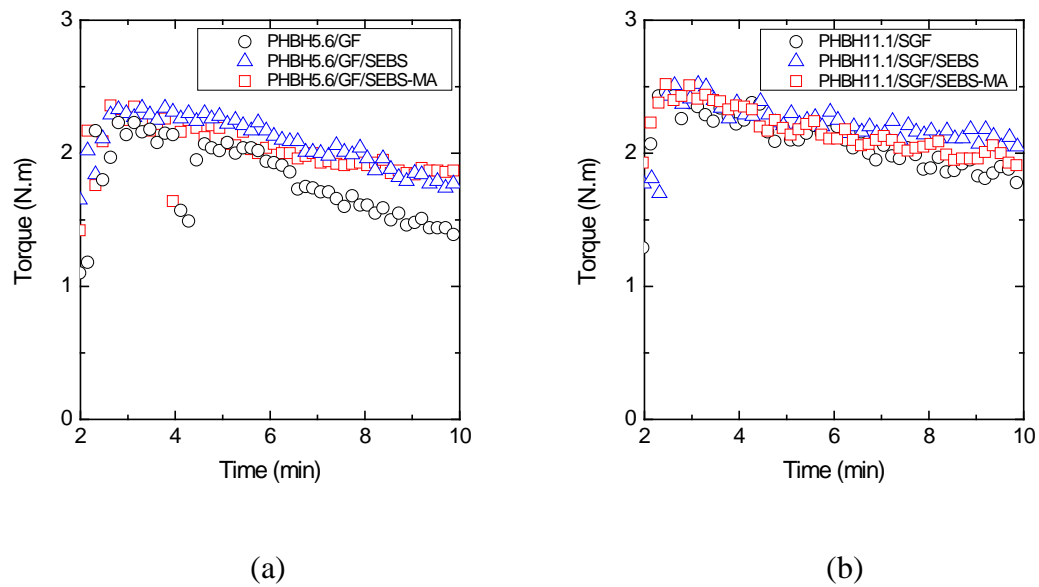


Figure 3.4 Torque versus time for (a) PHBH5.6/GF-based composites and (b) PHBH11.1/GF-based composites at the extruder barrel temperature of 150°C

The torque for pure SEBS and SEBS-MA as a function of time is shown in Figure 3.5. Neither of the thermoplastic elastomers could be processed at the extruder barrel temperature of 150°C due to their high viscosities. Therefore, the torque curves were obtained at the higher temperature of 220°C. The figure shows that the torque for SEBS is about two times higher than that for SEBS-MA. Nevertheless, the SEBS-based and SEBS-MA-based composites had similar torque values (Figure 3.4a and Figure 3.4b). This finding might be due to SEBS-MA having better adhesion with glass fibers than SEBS, as will be discussed later together with descriptions of fracture surface SEM observations. Similar phenomena were observed in PP/mica composites [30].

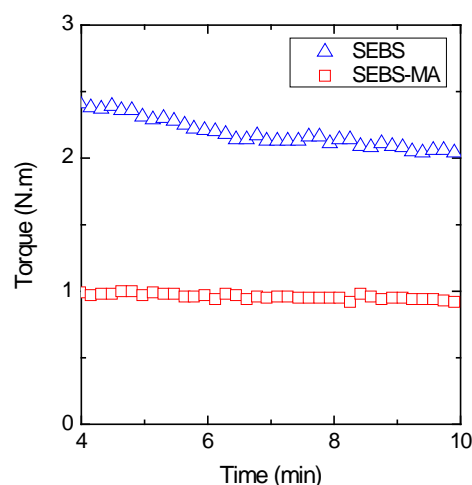


Figure 3.5 Torque versus time for SEBS and SEBS-MA at the extruder barrel temperature of 220°C

It is also noted that the average fiber length of PHBH5.6 was slightly longer than that of PHBH11.1 (see Figure 3.3). The relative difference in average fiber length is most likely due to PHBH11.1 having a relatively higher molecular weight and, thereby, greater viscosity than PHBH5.6 [14].

3.3.2 Tensile properties

Figure 3.6 illustrates typical stress–strain curves of PHBH5.6/GF-based composites (Figure 3.6a) and PHBH11.1/GF-based composites (Figure 3.6b) from tensile tests. The curves were obtained from PHBH/GF composites without thermoplastic elastomers (i.e. neat PHBH/GF composites), with SEBS, and with SEBS-MA. Comparing the tensile test results of PHBH/GF composites having different matrices (i.e., PHBH5.6 vs. PHBH11.1), it was found that PHBH5.6/GF composites had higher Young's modulus and strength but lower ductility than PHBH11.1/GF composites. This result agrees with those reported previously [14], in which PHBH gets softer and more flexible with the increase of 3HH content [11]. As to be discussed below, the addition of SEBS and SEBS-MA also has effects on tensile properties of PHBH/GF composites, but in a different manner.

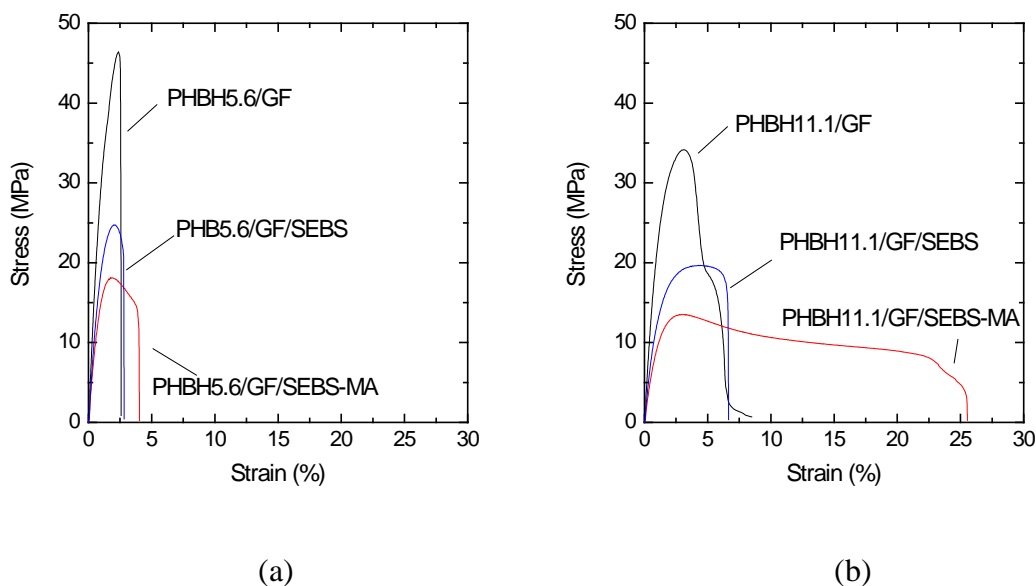
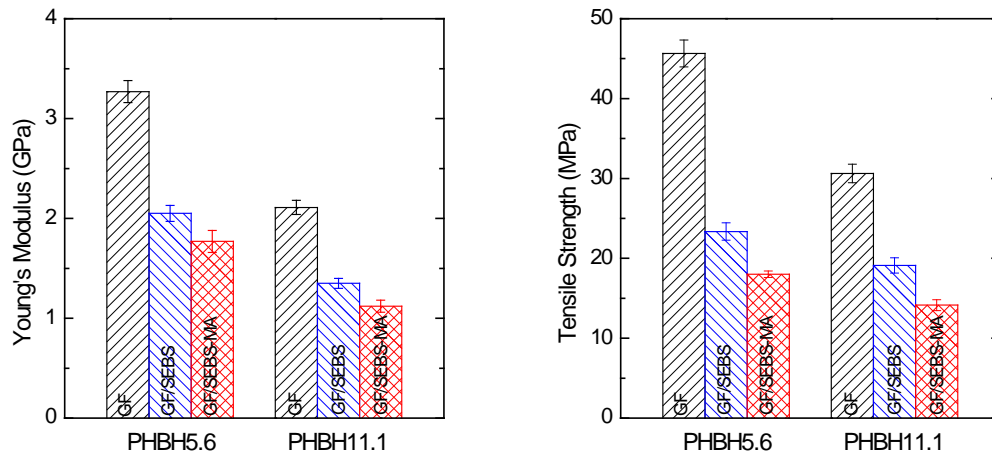


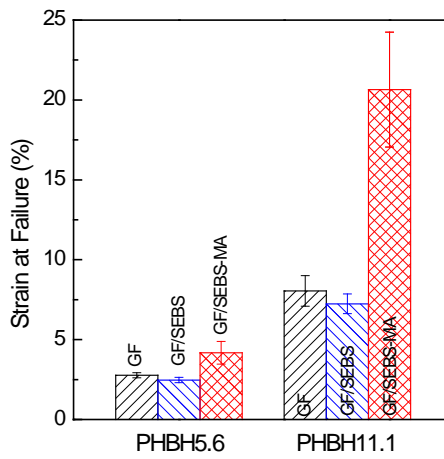
Figure 3.6 Stress-strain curves of (a) PHBH5.6/GF-based composites and (b) PHBH11.1/GF-based composites

Figure 3.7 summarizes the tensile properties of PHBH/GF composites without thermoplastic elastomers, with SEBS, and with SEBS-MA. Young's modulus is shown in Figure 3.7a. The Young's modulus of both PHBH5.6/GF and PHBH11.1/GF composites decreased with the addition of SEBS and SEBS-MA, but the Young's modulus of SEBS-based PHBH/GF composites was higher than that of SEBS-MA-based PHBH/GF composites. Figure 3.7b shows strength. Similar to the trend found in the Young's modulus, the addition of SEBS and SEBS-MA decreased the strength of both PHBH5.6/GF and PHBH11.1/GF composites, and strength of SEBS-based PHBH/GF composites was higher than that of their SEBS-MA-based counterparts. Figure 3.7c shows strain at failure. The addition of SEBS had little effect on failure strain of both PHBH5.6/GF and PHBH11.1/GF composites, but the addition of SEBS-MA significantly increased the failure strain of both PHBH5.6/GF and PHBH11.1/GF composites.



(a)

(b)



(c)

Figure 3.7 Mechanical properties of PHBH/GF composites without thermoplastic elastomers, with SEBS, and with SEBS-MA: (a) Young's modulus, (b) Strength, and (c) Strain at failure

Photographs of specimens after tensile tests under transmitted light are presented in Figure 3.8. The stress-whitening zone, which is a phenomenon generated from the plastic deformation and appears to be darker than the un-deformed region due to opacity of the zone, can be observed in PHBH/GF composites. Comparing the stress-whitening zones of PHBH5.6/GF and PHBH11.1/GF composites without thermoplastic elastomers, it can be seen that a small number of stress-whitening bands were developed in PHBH5.6/GF composites, whereas many stress-whitening bands were generated in PHBH11.1/GF composites. The addition of SEBS and SEBS-MA had little effect on the number of stress-whitening bands for both PHBH5.6/GF and PHBH11.1/GF composites. However, SEBS-MA created more stress-whitening bands as well as a large stress-whitening zone near the fracture surface. The variation of total size of stress-whitening zone is qualitatively consistent with the variation of the failure strain.

Figure 3.9 demonstrates fracture energy, which is defined by the area enclosed by the load-displacement curve, of the PHBH/GF composites without thermoplastic elastomers, with SEBS, and with SEBS-MA. The addition of SEBS and SEBS-MA decreased the fracture energy of PHBH5.6/GF composites, with the fracture energy with SEBS-MA being higher than that with SEBS. The decrease in the fracture energy of PHBH5.6/GF composites by the SEBS and SEBS-MA addition was mainly due to the decrease of tensile strength (see Figure 3.7b). On the other hand, for PHBH11.1/GF composites, the addition of SEBS decreased fracture energy, but the addition of SEBS-MA increased fracture energy. Although the SEBS and SEBS-MA addition decreased tensile strength (see Figure 3.7b), the SEBS-MA addition significantly increased failure strain (see

Figure 3.7c). As a result, the SEBS-MA addition increased fracture energy of PHBH11.1/GF composites, which will be further discussed below.

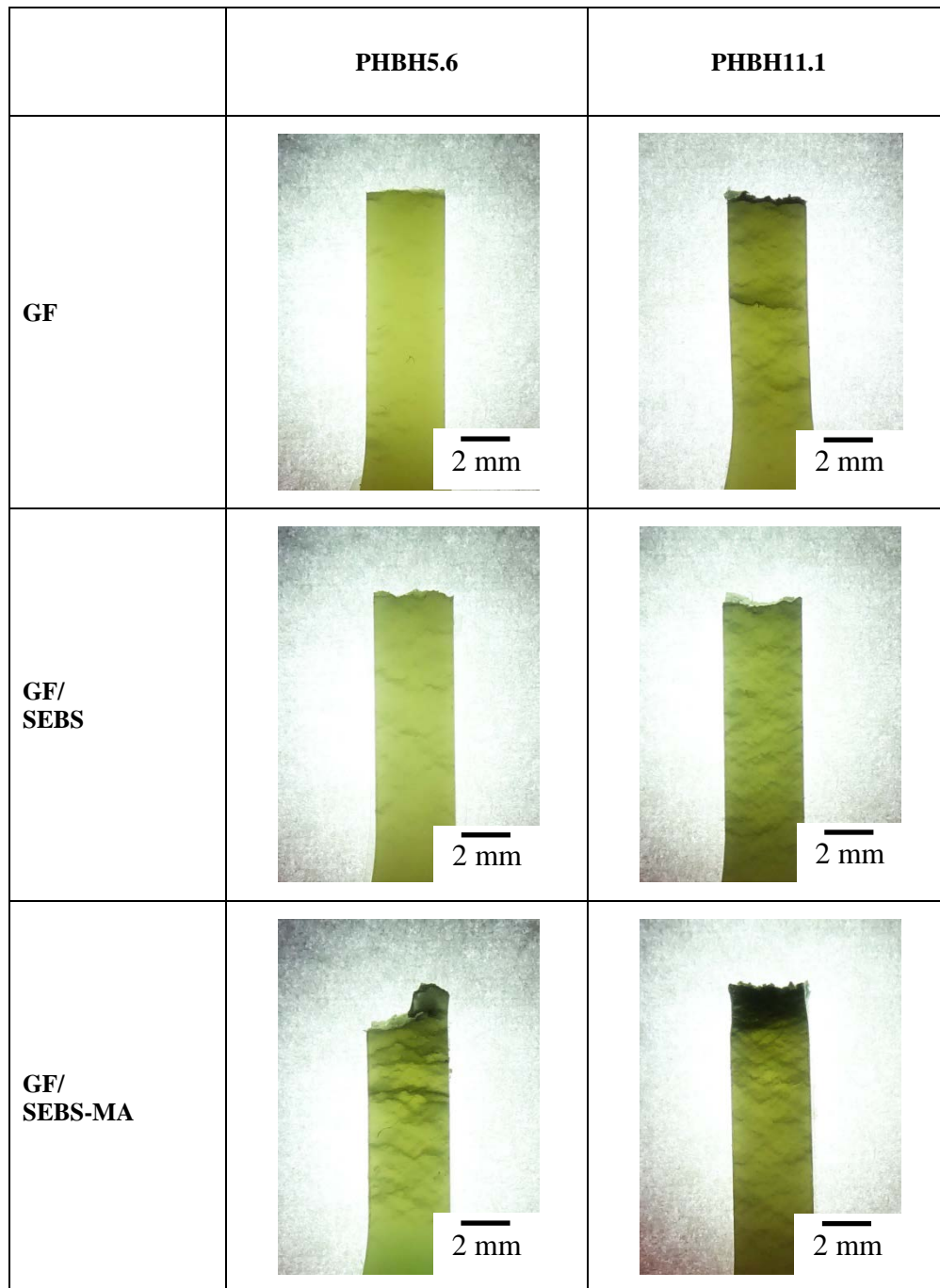


Figure 3.8 Photographs of PHBH/GF composite specimens after tensile tests under transmitted light

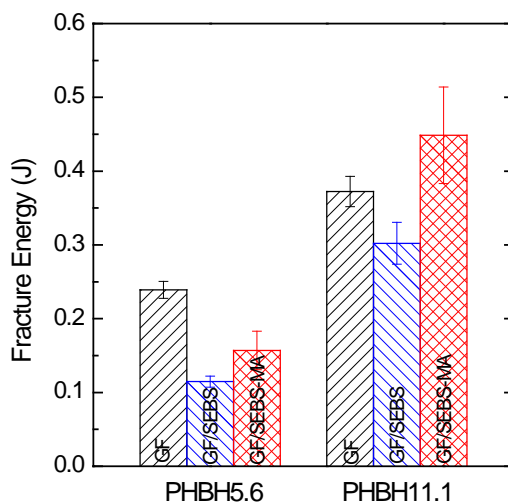


Figure 3.9 Fracture energy of PHBH/GF composites without thermoplastic elastomers, with SEBS, and with SEBS-MA

Figure 3.10 provides representational SEM micrographs of tensile specimen fracture surfaces. A comparison between fracture surfaces of PHBH5.6/GF and PHBH11.1/GF composites without thermoplastic elastomers shows that they are similar in fiber behavior but different in PHBH matrix behavior. Both composites show fiber fracture and fiber pullout, with the fiber surface being very smooth. The fracture surface of the PHBH matrix, however, is flatter and smoother in PHBH5.6/GF composites than in PHBH11.1/GF composites. Additionally, PHBH5.6/GF composites have little plastic deformation around fibers, whereas PHBH11.1/GF composites show considerable plastic deformation around fibers.

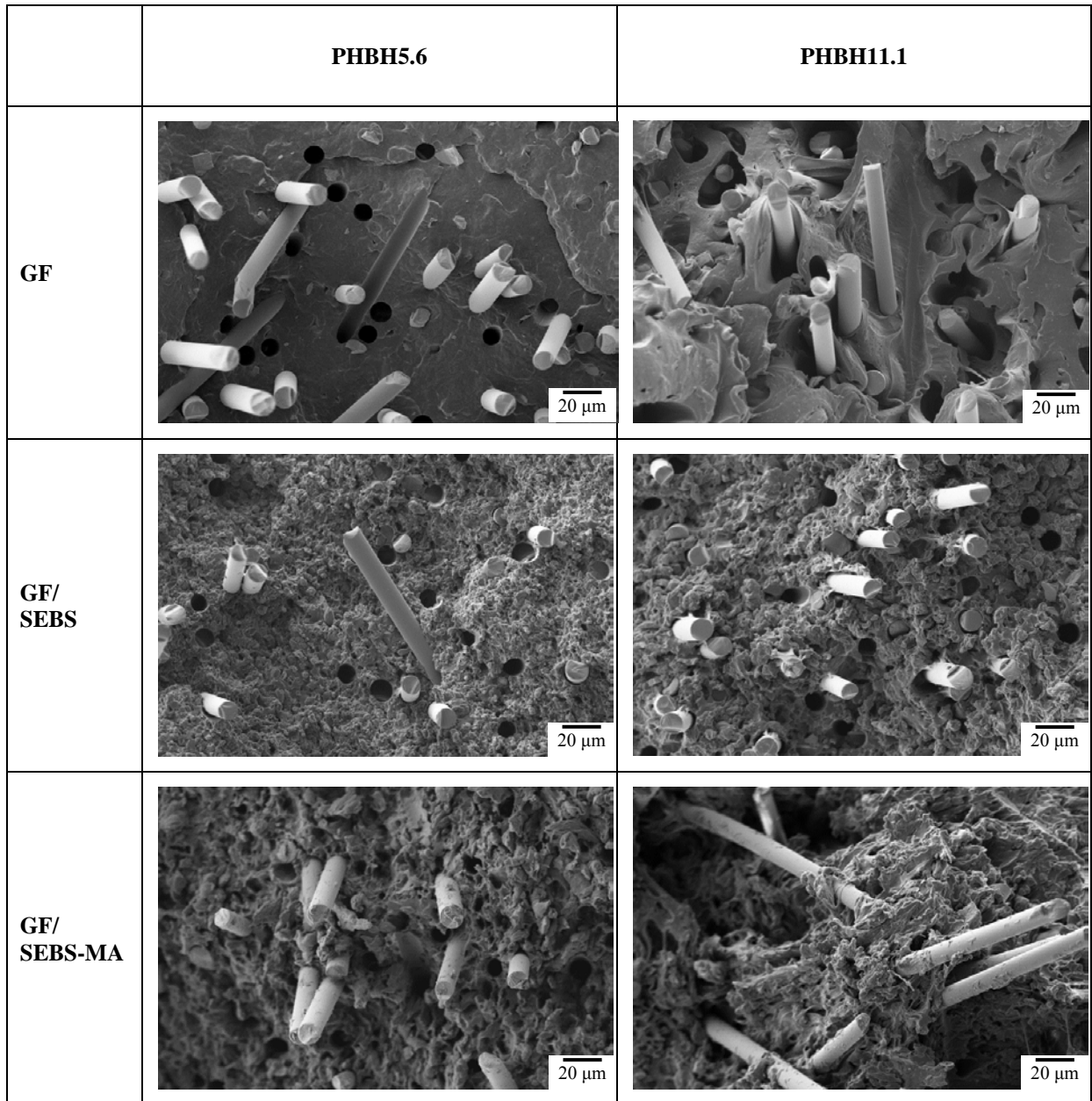


Figure 3.10 SEM images of fracture surface of PHBH/GF composite specimens after tensile test

When SEBS and SEBS-MA were added to PHBH5.6/GF and PHBH11.1/GF composites, fine particles, uniformly dispersed in the PHBH matrix, were observed on the fracture surface, and it is surmised that the particles are SEBS or SEBS-MA phase. However, there was a difference in fiber surface between the SEBS-based and SEBS-MA-based

PHBH/GF composites. In SEBS-based PHBH/GF composites, the surface of most of the fibers was smooth, which is the same phenomenon as was observed in PHBH/GF composites without thermoplastic elastomers. In contrast, SEBS-MA-based PHBH/GF composites had polymer portions adhering to fibers. These phenomena could be explained as follows: the maleic anhydride (MA) groups, which grafted to the central ethylene-butylene (EB) chain segment in the SEBS-MA, reacted with the hydroxyl groups (OH) on the surface of the glass fibers such that ester bonding and/or hydrogen bonding occurred between SEBS-MA and glass fibers during compounding. As a result, SEBS-MA bonded with (i.e. adhered to) glass fibers, thereby forming a rubbery interfacial layer between glass fibers and PHBH matrix. In other words, glass fibers were encapsulated by SEBS-MA. However, encapsulation of glass fibers by SEBS was neither observed nor expected, because of the absence of the MA groups in SEBS. Glass fibers were in direct contact with both PHBH matrix and SEBS. The SEBS-MA encapsulation of glass fibers prevented microcracks generated at the fiber interface from propagating through the PHBH matrix, thus providing higher failure strain of the composites. This increase led to superior fracture energy and, as to be discussed in the next section, notched Izod impact strength.

3.3.3 Notched Izod impact strength

Figure 3.11 depicts notched Izod impact strength of the PHBH/GF composites without thermoplastic elastomers, with SEBS, and with SEBS-MA. For PHBH5.6/GF-based composites, the notched Izod impact strength was little affected by the addition of SEBS, but was increased by the addition of SEBS-MA. For PHBH11.1/GF-based composites, the notched Izod impact strength was increased significantly by both SEBS and SEBS-MA addition, with SEBS-MA-based composites having higher notched Izod impact strength than SEBS-based composites.

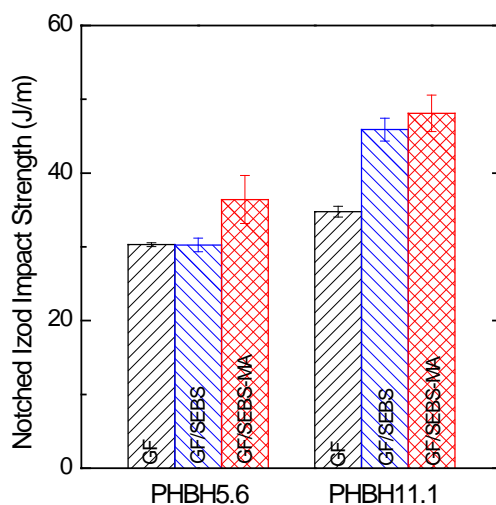


Figure 3.11 Notched Izod impact strength of PHBH/GF composites without thermoplastic elastomers, with SEBS, and with SEBS-MA

Photographs of specimens after notched Izod impact tests under transmitted light are presented in Figure 3.12. The top surface of the specimen is the fracture surface. The notch is located on the left of the specimen and the crack propagated from the left to the right. Unlike the tensile specimens, no distinct stress-whitening zone was observed in any of the PHBH/GF composites. However, the fracture surface of PHBH/GF composites with SEBS and SEBS-MA is more curved and rougher than that of the neat PHBH/GF composites.

Figure 3.13 shows representational SEM micrographs of fracture surfaces of notched Izod impact specimens. Both PHBH5.6/GF and PHBH11.1/GF composites without thermoplastic elastomers showed fiber fracture and fiber pullout, with the surface of fiber being very smooth, as well as brittle fracture surface (i.e., flat and smooth) of the PHBH matrix. The addition of SEBS and SEBS-MA created very rough fracture surface for both PHBH5.6/GF and PHBH11.1/GF composites. Moreover, polymer portions adhered to fibers in both SEBS-MA-based PHBH5.6/GF and PHBH11.1/GF composites. It is expected that, due to stress concentration, plastic deformation around SEBS and SEBS-MA particles occurred in the region ahead of the crack. Therefore, compared with PHBH/GF composites without thermoplastic elastomers, the thermoplastic elastomer-containing PHBH/GF composites had more plastic energy absorbed and rough fracture surface was generated. Furthermore, SEBS-MA encapsulated glass fibers and thus prevented microcracks generated at the fiber interface from propagating through the PHBH matrix.

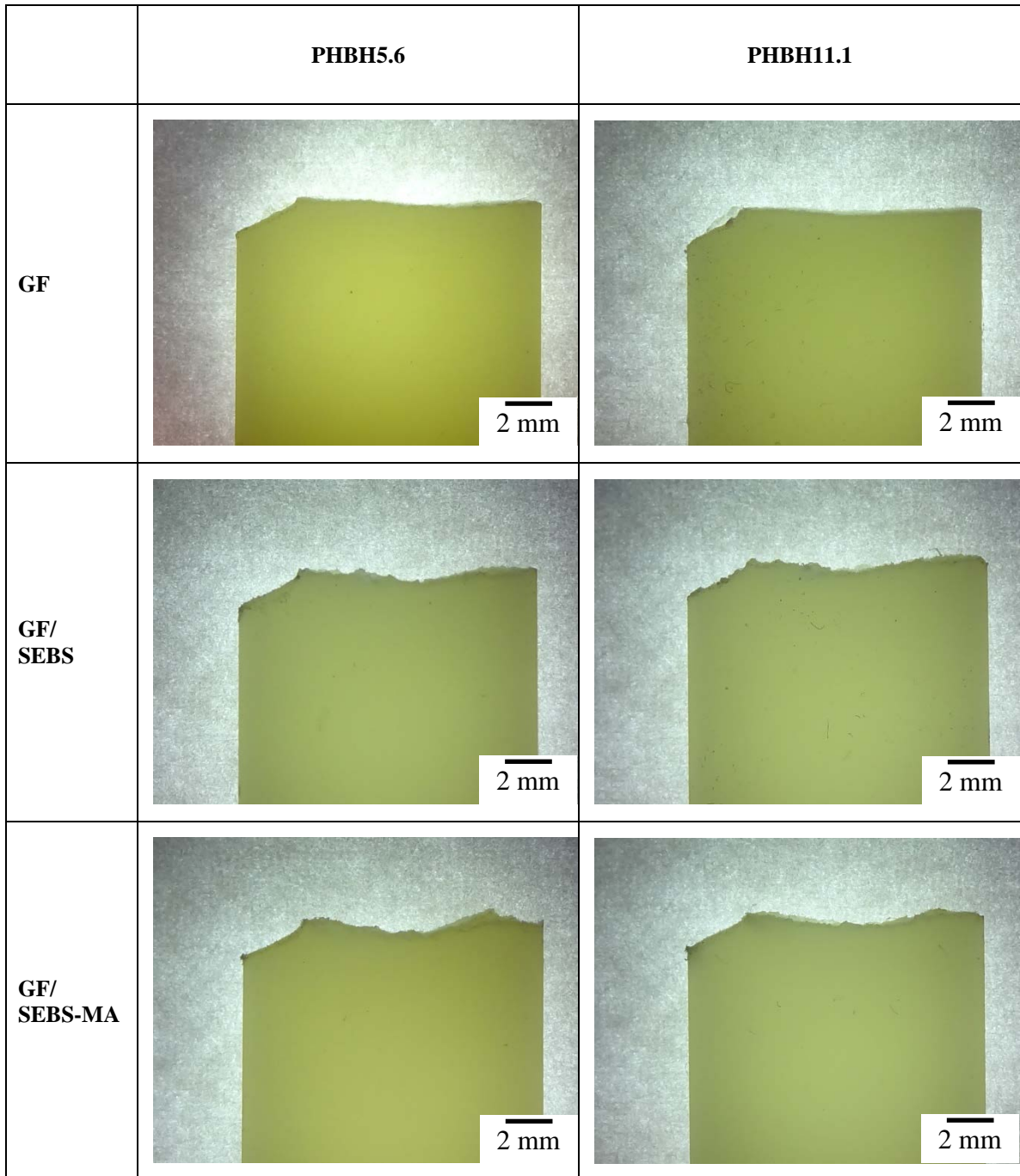


Figure 3.12 Photographs of PHBH/GF composite specimens after notched Izod impact tests under transmitted light

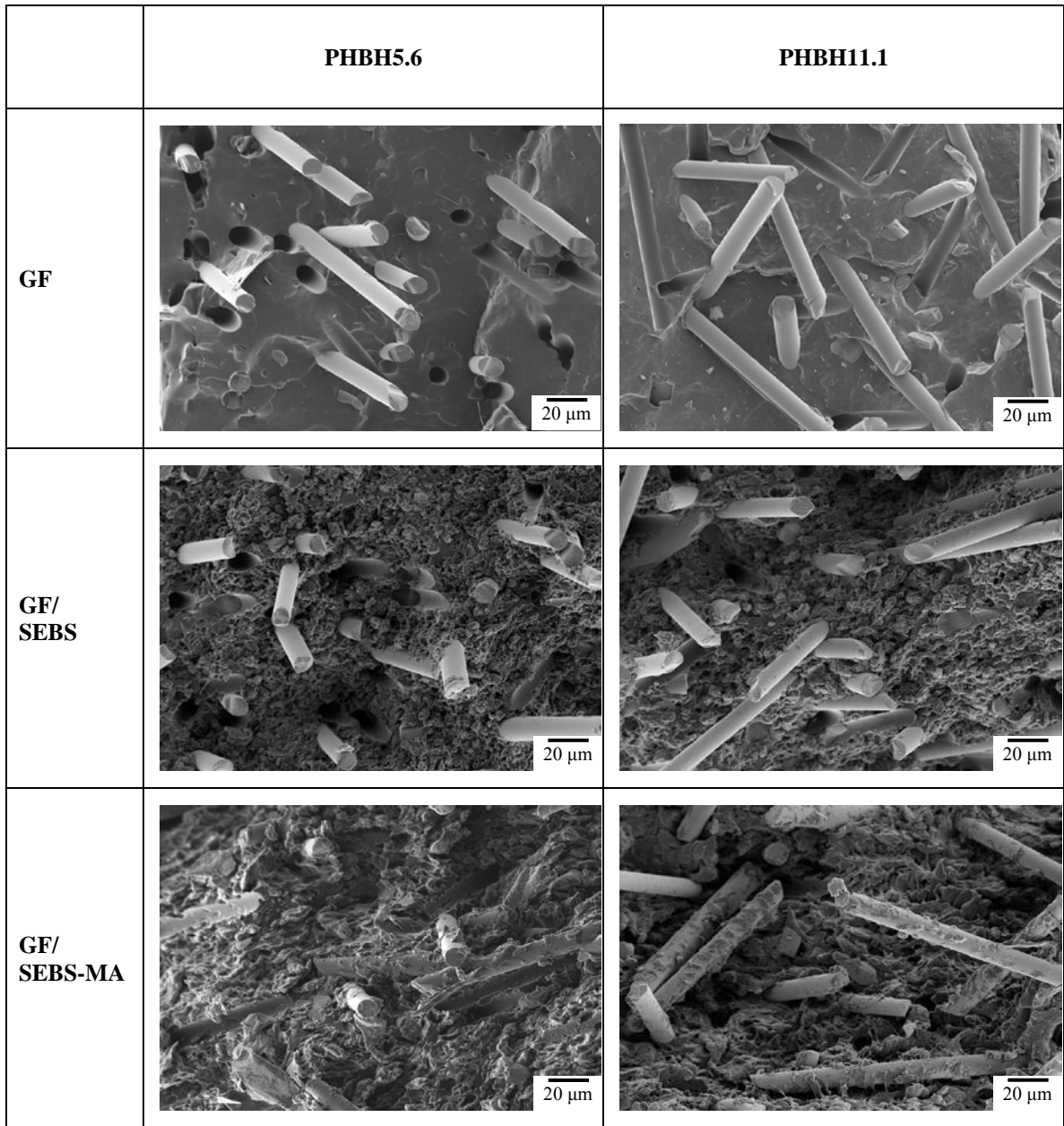


Figure 3.13 SEM images of fracture surface of PHBH/GF composites after notched Izod impact tests

As tensile testing showed, the addition of SEBS and SEBS-MA decreased fracture energy of the PHBH/GF composites in all cases except that of PHBH11.1/GF/SEBS-MA, in which fracture energy was increased (see Figure 3.9). In contrast, the addition of SEBS and SEBS-MA increased the notched Izod impact strength of the PHBH/GF composites in all cases except that of PHBH5.6/GF/SEBS composites, in which notched Izod impact strength was little affected (see Figure 3.11). The fracture energy measured from tensile tests differs from notched Izod impact strength mainly in three aspects: absence of notch in a specimen, use of tensile loading rather than flexural loading, and lower strain rate [31]. One explanation for why the effects of the thermoplastic elastomers on fracture energy were different from those on notched Izod impact strength could be that the addition of SEBS and SEBS-MA decreased the energy needed for crack initiation, but increased the energy needed for crack propagation of PHBH/GF composites. The fracture energy measured from tensile tests includes the energy needed for both crack initiation and crack propagation but, for the composite materials manufactured in this study, energy needed for crack initiation contributed to fracture energy more than did energy needed for crack propagation. As a result, the addition of SEBS and SEBS-MA decreased fracture energy. In contrast, because notched Izod impact strength is more associated with crack propagation, the addition of SEBS and SEBS-MA increased notched Izod impact strength. Nevertheless, further study is needed to test this speculation as well as the effects of loading mode (tensile vs. flexural) and strain rate.

3.3.4 Thermal properties

Figure 3.14 and Figure 3.15 depict the first and second DSC heating curves of, respectively, PHBH5.6/GF (Figure 3.14a and Figure 3.15a) and PHBH11.1/GF (Figure 3.14b and Figure 3.15b) composites without thermoplastic elastomers, with SEBS, and with SEBS-MA. All composites showed two melting temperatures: T_{m1} and T_{m2} , where $T_{m1} < T_{m2}$. The melting temperature T_{m1} is related to the melting of crystals formed originally during the cooling process and annealing at room temperature, whereas the melting temperature T_{m2} is associated with the melting of crystals that were re-crystallized during the heating process [32–36]. All PHBH11.1/GF-based composites also had another melting temperature T_a , lower than T_{m1} and T_{m2} , on the first heating curves (Figure 3.14b), but not on the second heating curves (Figure 3.15b) due to the absence of an annealing period at room temperature between the cooling and second heating scans. The melting temperature T_a originates from the melting of small imperfect crystallites that form during annealing at room temperature [14,34–36].

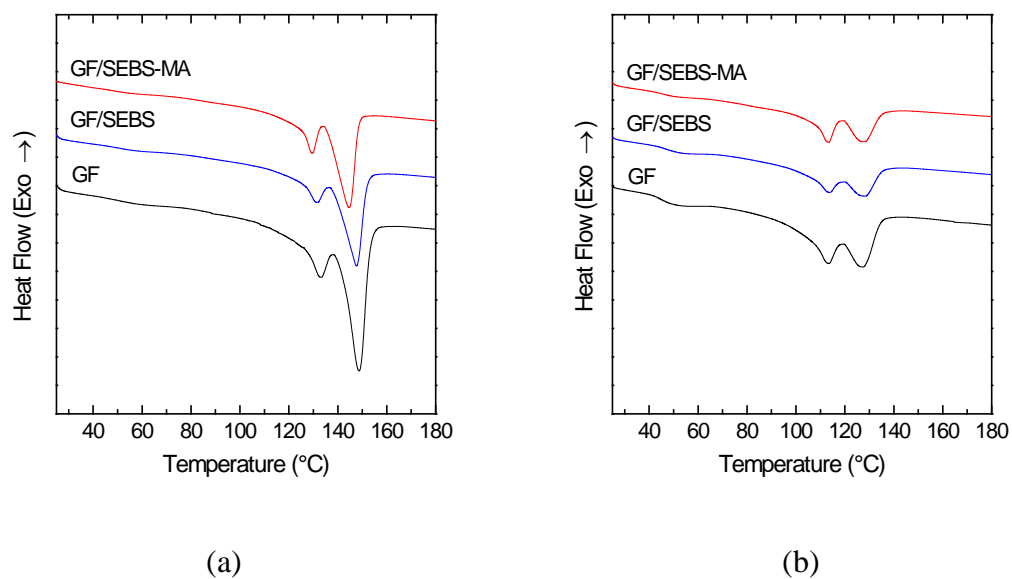


Figure 3.14 First DSC heating curves of (a) PHBH5.6/GF-based composites and (b) PHBH11.1/GF-based composites

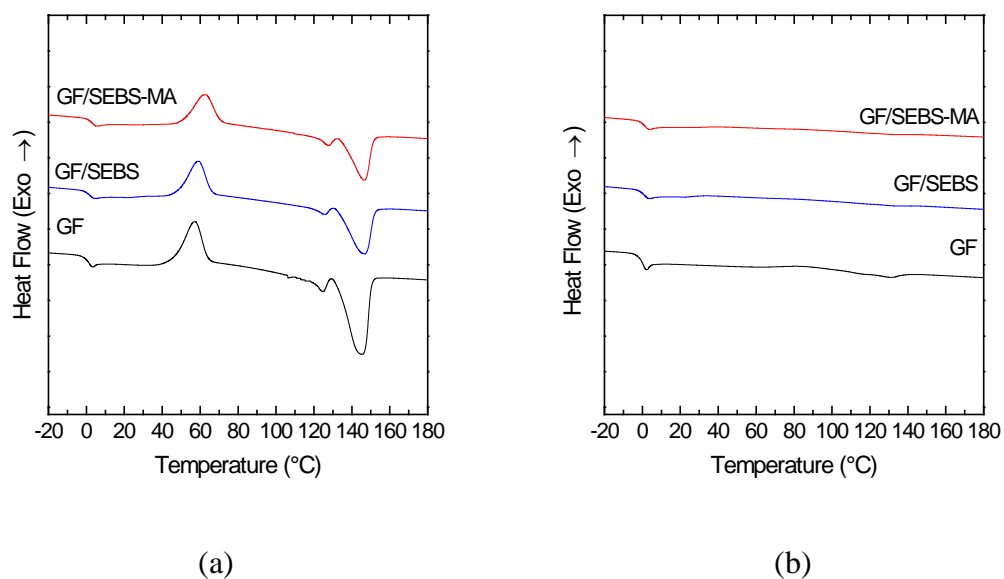


Figure 3.15 Second DSC heating curves of (a) PHBH5.6/GF-based composites and (b) PHBH11.1/GF-based composites

Degree of crystallinity X_c of injection molded tensile specimens was calculated from the first and second heating DSC curves and the following equation:

$$X_c = \frac{\Delta H_m - \Delta H_{cc}}{\Delta H_f(1 - W_f - W_{TE})} \times 100\% \quad (1)$$

where ΔH_m is enthalpy of fusion; ΔH_{cc} is enthalpy of cold crystallization; ΔH_f is enthalpy of fusion of fully crystalline PHB, which is taken to be 146 J/g [37]; W_f is the weight fraction of fiber; and W_{TE} is the weight fraction of thermoplastic elastomer.

The thermal properties obtained from the first and second DSC heating curves are summarized in Table 3.2 and Table 3.3, respectively. The tables show that PHBH5.6/GF-based composites had higher melting temperatures T_{m1} and T_{m2} , as well as higher degree of crystallinity X_c than PHBH11.1/GF-based composites, which suggests that the secondary comonomer unit 3HH disturbed the poly(3-hydroxybutyrate)-type crystal lattice and suppressed crystallization [33]. Additionally, the degree of crystallinity X_c obtained from the first heating curves (Figure 3.14) was higher than that obtained from the second heating curves (Figure 3.15), which suggests that secondary crystallization occurred during solidification in injection molding and during the two days of annealing at room temperature.

Table 3.2, summarizing data obtained from the first DSC heating curves, demonstrates that the both SEBS and SEBS-MA addition reduced the degree of crystallinity of PHBH/GF composites. It may be reasonably presumed, therefore, that the reduction in degree of crystallinity contributed to some extent to the decrease in Young's modulus, decrease in tensile strength, and increase in ductility, observed in the PHBH/GF

composites with addition of SEBS or SEBS-MA. Table 3.3, summarizing data obtained from the second DSC heating curves, shows that both SEBS and SEBS-MA addition decreased degree of crystallinity of PHBH5.6/GF composites, but negligibly affected degree of crystallinity of PHBH11.1/GF composites. Table 3.2 and Table 3.3 also indicate that, in all PHBH/GF composites, both SEBS and SEBS-MA addition had little effect on glass transition temperature T_g , which suggests that neither SEBS nor SEBS-MA is miscible with PHBH/GF.

Table 3.2 Thermal properties of PHBH/GF/TE composites characterized from the first DSC curves

Sample	T_a (°C)	ΔH_a (J/g)	T_{m1} (°C)	T_{m2} (°C)	ΔH_m^{1st} (J/g)	X_c^{1st} (%)
PHBH5.6/GF	-	0.0	133.2	148.7	47.6	40.8
PHBH5.6/GF/SEBS	-	0.0	131.7	147.5	24.8	34.0
PHBH5.6/GF/SEBS-MA	-	0.0	129.5	144.4	24.7	33.9
PHBH11.1/GF	51.2	1.2	113.1	127.6	32.8	29.1
PHBH11.1/GF/SEBS	52.7	0.5	114.0	128.3	19.9	27.9
PHBH11.1//GF/SEBS-MA	50.4	0.3	113.1	127.5	19.3	26.9

Table 3.3 Thermal properties of PHBH/GF/TE composites characterized from the second DSC heating curves

Sample	T_g (°C)	T_{cc} (°C)	T_{m1} (°C)	T_{m2} (°C)	ΔH_{cc} (J/g)	ΔH_m^{2nd} (J/g)	X_c^{2nd} (%)
PHBH5.6/GF	0.9	57.2	124.6	144.9	23.3	47.1	20.4
PHBH5.6/GF/SEBS	1.5	59.2	126.2	146.0	16.0	26.6	14.5
PHBH5.6/GF/SEBS-MA	2.0	59.4	126.5	145.3	15.6	25.4	13.5
PHBH11.1/GF	-0.6	83.7	115.6	129.9	2.0	3.2	1.0
PHBH11.1/GF/SEBS	0.3	82.2	115.8	133.2	0.3	1.4	1.5
PHBH11.1//GF/SEBS-MA	0.9	84.4	116.7	133.8	0.4	1.0	0.9

Figure 3.16 illustrates DSC cooling curves of PHBH5.6/GF (Figure 3.16a) and PHBH11.1/GF (Figure 3.16b) composites without thermoplastic elastomers, with SEBS, and with SEBS-MA. PHBH5.6/GF-based composites showed crystallization temperature while PHBH11.1/GF-based composites did not, because the crystallization rate decreased with the increase of 3HH content. It is noted that two crystallization peaks (45.2 and 55.6°C) appeared in PHBH5.6/GF/SEBS-MA composites. Further study is needed to investigate these peaks.

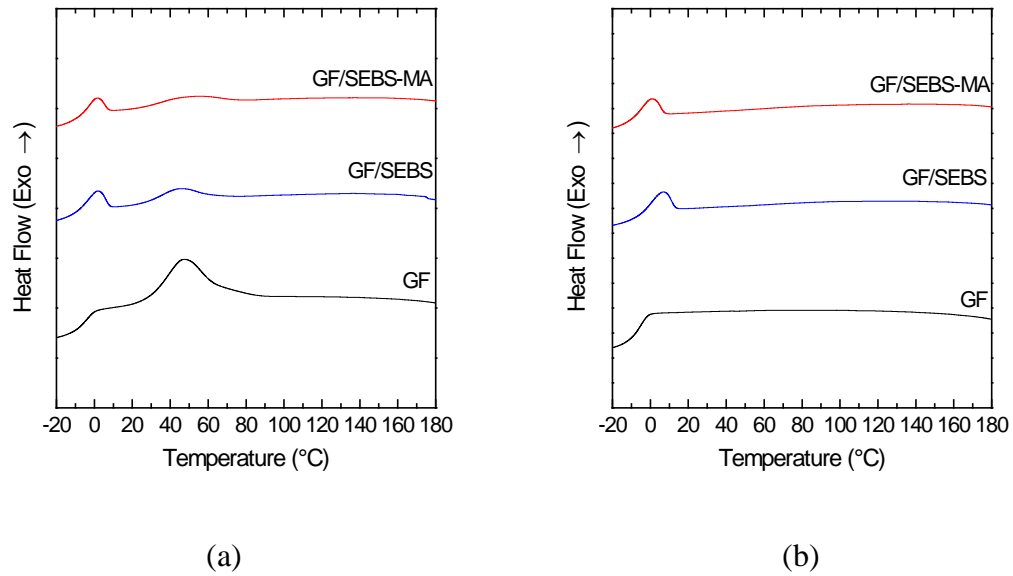


Figure 3.16 DSC cooling curves of (a) PHBH5.6/GF-based composites and (b) PHBH11.1/GF-based composites

3.3.5 Non-isothermal crystallization kinetics

Because no crystallization temperature was observed in PHBH11.1/GF composites, regardless of whether it contained SEBS, SEBS-MA, or neither; crystallization kinetics of only PHBH5.6/GF-based composites were analyzed. The relative degree of crystallinity as a function of temperature can be calculated using the DSC cooling curves and the following equation [38]:

$$X(T) = \frac{\int_{T_0}^T \left(\frac{dH_c}{dT} \right) dT}{\int_{T_0}^{T_\infty} \left(\frac{dH_c}{dT} \right) dT} \quad (2)$$

where T_0 and T_∞ represent onset and end-crystallization temperatures, respectively.

Crystallization kinetics under isothermal conditions are often analyzed using the following Avrami equation [39]:

$$X(t) = 1 - \exp(-z_t t^n) \quad (3)$$

where $X(t)$ is the relative degree of crystallinity, n is the Avrami exponent that depends on the nature of the nucleation mechanism and growth geometry of crystals, z_t is the crystallization rate constant that involves both nucleation and growth rate parameters, and t is the time.

In non-isothermal crystallization processes, the relationship between crystallization time t and temperature T is given by:

$$t = \frac{|T_0 - T|}{\phi} \quad (4)$$

By taking into account the time-temperature relationship of equation 5, equation 4 can be transformed into the double-logarithmic form,

$$\log[-\ln(1 - X(T))] = \log Z_t + n \log t \quad (5)$$

The parameters n (slope) and Z_t (intercept) were determined by plotting $\log[-\ln(1 - X(T))]$ against $\log t$.

Jeziorny [40] pointed out that the composite rate constant z_t should be adequately corrected to take into account the cooling rate of the polymer. Assuming constant cooling rate ϕ , the parameter characterizing kinetics of non-isothermal crystallization was given as follows:

$$\log Z_c = \frac{\log Z_t}{\phi} \quad (6)$$

The crystallization half-time $t_{1/2}$, which is defined as the time taken from the onset of the crystallization until 50% completion, was calculated as follows:

$$t_{1/2} = \left(\frac{\ln 2}{Z_c} \right)^{\frac{1}{n}} \quad (7)$$

Figure 3.17 shows Avrami plots, i.e., plots of $\log[-\ln(1 - X(T))]$ versus $\log t$, of PHBH5.6 /GF composites without thermoplastic elastomers, with SEBS, and with SEBS-MA. All of the composites showed a linear line and there was no significant shift of the lines. Kinetic parameters determined by the Avrami equation with Jeziorny's correction are summarized in Table 3.4. The addition of SEBS and SEBS-MA did not affect the crystallization half-time of PHBH5.6/GF though the addition of SEBS and SEBS-MA decreased the degree of crystallinity (Table 3.2 and Table 3.3).

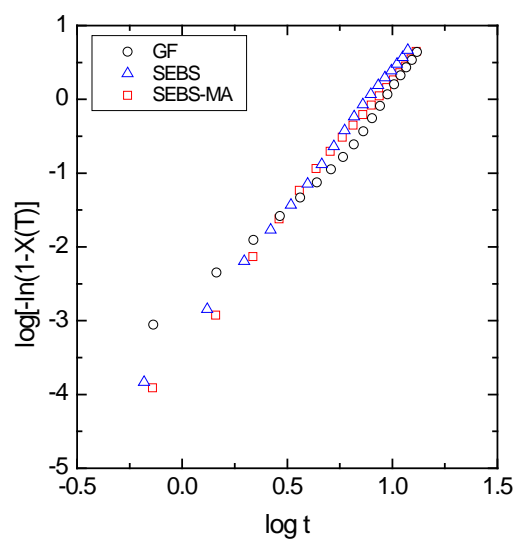


Figure 3.17 Avrami plots of PHBH5.6/GF-based composites

Table 3.4 Thermal properties of PHBH5.6/GF/TE composites characterized from the DSC cooling curves and non-isothermal kinetic parameters calculated from the modified Avrami equation

Sample	T_o (°C)	T_c (°C)	ΔC_c (J/g)	Z_c	n	$t_{1/2}$ (min)
PHBH5.6/GF	90.5	46.9	13.6	0.26	3.00	1.38
PHBH5.6/GF/SEBS	76.8	46.1	3.6	0.22	3.66	1.36
PHBH5.6/GF/SEBS-MA	83.1	45.2, 55.6	3.1	0.21	3.63	1.38

3.4 Conclusions

The effects of thermoplastic elastomers (TE), SEBS and SEBS-MA, on the mechanical and thermal properties of PHBH/GF composites were investigated. Mechanical test results suggested that the addition of SEBS did not increase the tensile failure strain of PHBH/GF composites while the addition of SEBS-MA significantly increased the tensile failure strain of PHBH/GF composites. Fracture energy, defined by the area enclosed by the load-displacement curve under tensile test, and notched Izod impact strength of PHBH/GF/TE composites were measured to evaluate their energy absorption capability in fracture. The effects of SEBS and SEBS-MA on fracture energy in tensile tests were different from their effects on notched Izod impact strength. The addition of SEBS and SEBS-MA decreased fracture energy of all PHBH/GF composites except PHBH11.1/GF/SEBS-MA composites. In contrast, the addition of SEBS and SEBS-MA increased notched Izod impact strength of all PHBH/GF composites except PHBH5.6/GF/SEBS composites. Nevertheless, SEBS-MA was more effective in the energy absorption than SEBS, presumably due to its difference in morphology; that is, SEBS-MA encapsulated fibers as well as dispersed in the PHBH matrix, whereas SEBS dispersed in the PHBH matrix without fiber encapsulation. DSC results suggested that both SEBS and SEBS-MA addition decreased the degree of crystallinity of PHBH/GF composites. However, analysis of non-isothermal crystallization kinetics of PHBH5.6/GF composites, using the modified Avrami equation, showed that both SEBS and SEBS-MA addition had little effect on crystallization half-time.

3.5 Reference

- [1] Philip S, Keshavarz T, Roy I. Polyhydroxyalkanoates: biodegradable polymers with a range of applications. *J Chem Technol Biotechnol* 2007;82:233–47. doi:10.1002/jctb.1667.
- [2] Chen G-Q. A microbial polyhydroxyalkanoates (PHA) based bio- and materials industry. *Chem Soc Rev* 2009;38:2434–46.
- [3] Williams SF, Martin DP, Horowitz DM, Peoples OP. PHA applications: addressing the price performance issue. *Int J Biol Macromol* 1999;25:111–21. doi:10.1016/S0141-8130(99)00022-7.
- [4] Chen G-Q, Wu Q. The application of polyhydroxyalkanoates as tissue engineering materials. *Biomaterials* 2005;26:6565–78. doi:10.1016/j.biomaterials.2005.04.036.
- [5] Lee SY. Bacterial polyhydroxyalkanoates. *Biotechnol Bioeng* 1996;49:1–14. doi:10.1002/(SICI)1097-0290(19960105)49:1<1::AID-BIT1>3.0.CO;2-P.
- [6] Madison LL, Huisman GW. Metabolic Engineering of Poly(3-Hydroxyalkanoates): From DNA to Plastic. *Microbiol Mol Biol Rev* 1999;63:21–53.
- [7] Wang Y, Yin J, Chen G-Q. Polyhydroxyalkanoates, challenges and opportunities. *Curr Opin Biotechnol* 2014;30:59–65. doi:10.1016/j.copbio.2014.06.001.

- [8] Noda I, Green PR, Satkowski MM, Schechtman LA. Preparation and properties of a novel class of polyhydroxyalkanoate copolymers. *Biomacromolecules* 2005;6:580–6. doi:10.1021/bm049472m.
- [9] Sudesh K, Abe H, Doi Y. Synthesis, structure and properties of polyhydroxyalkanoates: biological polyesters. *Prog Polym Sci* 2000;25:1503–55. doi:10.1016/S0079-6700(00)00035-6.
- [10] Laycock B, Halley P, Pratt S, Werker A, Lant P. The chemomechanical properties of microbial polyhydroxyalkanoates. *Prog Polym Sci* 2013;38:536–83. doi:10.1016/j.progpolymsci.2012.06.003.
- [11] Doi Y, Kitamura S, Abe H. Microbial Synthesis and Characterization of Poly(3-hydroxybutyrate-co-3-hydroxyhexanoate). *Macromolecules* 1995;28:4822–8. doi:10.1021/ma00118a007.
- [12] Alata H, Aoyama T, Inoue Y. Effect of Aging on the Mechanical Properties of Poly(3-hydroxybutyrate-co-3-hydroxyhexanoate). *Macromolecules* 2007;40:4546–51. doi:10.1021/ma070418i.
- [13] Asrar J, Valentin HE, Berger PA, Tran M, Padgett SR, Garbow JR. Biosynthesis and properties of poly(3-hydroxybutyrate-co-3-hydroxyhexanoate) polymers. *Biomacromolecules* 2002;3:1006–12. doi:10.1021/bm025543a.
- [14] Arifin W, Kuboki T. Effects of Glass Fibers on Mechanical and Thermal Properties of Poly(3-hydroxybutyrate-co-3-hydroxyhexanoate) 2015:in preparation.

- [15] Tjong SC, Xu S-A, Li RK-Y, Mai Y-W. Mechanical behavior and fracture toughness evaluation of maleic anhydride compatibilized short glass fiber/SEBS/polypropylene hybrid composites. *Compos Sci Technol* 2002;62:831–40. doi:10.1016/S0266-3538(02)00037-4.
- [16] Tjong SC, Xu SA, Yu Li RK, Mai YW. Preparation and performance characteristics of short-glass-fiber/maleated styrene-ethylene-butylene-styrene/polypropylene hybrid composites. *J Appl Polym Sci* 2002;86:1303–11. doi:10.1002/app.11095.
- [17] Garakani MM, Arefazar A, Nazockdast H. Study on morphological, rheological, and mechanical properties of PP/SEBS-MA/SGF hybrid composites. *J Appl Polym Sci* 2007;104:2704–10. doi:10.1002/app.25700.
- [18] Gupta AK, Srinivasan KR, Kumar PK. Glass fiber reinforced polypropylene/EPDM blends. II. Mechanical properties and morphology. *J Appl Polym Sci* 1991;43:451–62. doi:10.1002/app.1991.070430306.
- [19] Barbosa SE, Caplati NJ, Blanca CCB, Kenny JM. Processability and Mechanical Properties of Ternary Composites PP/EPDM/GF. *Polymer (Guildf)* 2000;21:377–86. doi:10.1002/pc.10196.
- [20] Jancar J. Yielding and impact behaviour of pp/sgf/epr ternary composites with controlled morphology. *J Mater Sci* 1996;31:3983–7. doi:10.1007/BF00352659.

- [21] Karayannidis GP, Bikiaris DN, Papageorgiou GZ, Bakirtzis V. Rubber toughening of glass fiber reinforced nylon-6,6 with functionalized block copolymer SEBS-g-MA. *Adv Polym Technol* 2002;21:153–63. doi:10.1002/adv.10023.
- [22] Laura D., Keskkula H, Barlow J., Paul D. Effect of rubber particle size and rubber type on the mechanical properties of glass fiber reinforced, rubber-toughened nylon 6. *Polymer (Guildf)* 2003;44:3347–61. doi:10.1016/S0032-3861(03)00221-0.
- [23] Laura DM, Keskkula H, Barlow JW, Paul DR. Effect of glass fiber surface chemistry on the mechanical properties of glass fiber reinforced, rubber-toughened nylon 6. *Polymer (Guildf)* 2002;43:4673–87. doi:10.1016/S0032-3861(02)00302-6.
- [24] Fu S-Y, Lauke B, Li RKY, Mai Y-W. Effects of PA6,6/PP ratio on the mechanical properties of short glass fiber reinforced and rubber-toughened polyamide 6,6/polypropylene blends. *Compos Part B Eng* 2005;37:182–90. doi:10.1016/j.compositesb.2005.05.018.
- [25] Laura DM, Keskkula H, Barlow JW, Paul DR. Effect of glass fiber and maleated ethylene-propylene rubber content on tensile and impact properties of Nylon 6. *Polymer (Guildf)* 2000;41:7165–74. doi:10.1016/S0032-3861(00)00049-5.
- [26] Nair S V., Shiao ML, Garrett PD. Fracture resistance of a glass-fibre reinforced rubber-modified thermoplastic hybrid composite. *J Mater Sci* 1992;27:1085–100. doi:10.1007/BF01197664.

- [27] Fung KL, Li RKY. Mechanical properties of short glass fibre reinforced and functionalized rubber-toughened PET blends. *Polym Test* 2006;25:923–31. doi:10.1016/j.polymertesting.2006.05.013.
- [28] Fan* RR, Zhou* LX, Li DX, Zhang DM, Wu M, Guo G. Preparation and Characterization of Composites Based on Poly (Butylene Succinate) and Poly (Lactic Acid) Grafted Tetracalcium Phosphate. *J Macromol Sci Part B* 2013;53:296–308. doi:10.1080/00222348.2013.810104.
- [29] Thomason JL. Micromechanical parameters from macromechanical measurements on glass reinforced polypropylene. *Compos Sci Technol* 2002;62:1455–68. doi:10.1016/S0266-3538(02)00097-0.
- [30] Yazdani H, Morshedian J, Khonakdar HA. Effect of maleated polypropylene and impact modifiers on the morphology and mechanical properties of PP/mica composites. *Polym Compos* 2006;27:614–20. doi:10.1002/pc.20237.
- [31] Chen B, Evans JRG. Impact strength of polymer-clay nanocomposites. *Soft Matter* 2009;5:3572. doi:10.1039/b902073j.
- [32] Watanabe T, He Y, Fukuchi T, Inoue Y. Comonomer Compositional Distribution and Thermal Characteristics of Bacterially Synthesized Poly(3-hydroxybutyrate-co-3-hydroxyhexanoate)s. *Macromol Biosci* 2001;1:75–83. doi:10.1002/1616-5195(20010301)1:2<75::AID-MABI75>3.0.CO;2-Q.
- [33] Feng L, Watanabe T, Wang Y, Kichise T, Fukuchi T, Chen G-Q, et al. Studies on Comonomer Compositional Distribution of Bacterial Poly(3-hydroxybutyrate - co

- 3-hydroxyhexanoate)s and Thermal Characteristics of Their Fractions. *Biomacromolecules* 2002;3:1071–7. doi:10.1021/bm0200581.
- [34] Hu Y, Zhang J, Sato H, Noda I, Ozaki Y. Multiple melting behavior of poly(3-hydroxybutyrate-co-3-hydroxyhexanoate) investigated by differential scanning calorimetry and infrared spectroscopy. *Polymer (Guildf)* 2007;48:4777–85. doi:10.1016/j.polymer.2007.06.016.
- [35] Ye H-M, Wang Z, Wang H-H, Chen G-Q, Xu J. Different thermal behaviors of microbial polyesters poly(3-hydroxybutyrate-co-3-hydroxyvalerate-co-3-hydroxyhexanoate) and poly(3-hydroxybutyrate-co-3-hydroxyhexanoate). *Polymer (Guildf)* 2010;51:6037–46. doi:10.1016/j.polymer.2010.10.030.
- [36] Ding C, Cheng B, Wu Q. DSC analysis of isothermally melt-crystallized bacterial poly(3-hydroxybutyrate-co-3-hydroxyhexanoate) films. *J Therm Anal Calorim* 2010;103:1001–6. doi:10.1007/s10973-010-1135-8.
- [37] Pan P, Liang Z, Nakamura N, Miyagawa T, Inoue Y. Uracil as nucleating agent for bacterial poly[(3-hydroxybutyrate)-co-(3-hydroxyhexanoate)] copolymers. *Macromol Biosci* 2009;9:585–95. doi:10.1002/mabi.200800294.
- [38] Barham PJ, Keller A, Otun EL, Holmes PA. Crystallization and morphology of a bacterial thermoplastic: poly-3-hydroxybutyrate. *J Mater Sci* 1984;19:2781–94. doi:10.1007/BF01026954.
- [39] Bianchi O, Oliveira RVB, Fiorio R, Martins JDN, Zattera AJ, Canto LB. Assessment of Avrami, Ozawa and Avrami–Ozawa equations for determination of

EVA crosslinking kinetics from DSC measurements. *Polym Test* 2008;27:722–9.
doi:10.1016/j.polymertesting.2008.05.003.

[40] Avrami M. Kinetics of phase change. I: General theory. *J Chem Phys* 1939;7:1103–12.

[41] Jeziorny A. Parameters characterizing the kinetics of the non-isothermal crystallization of poly(ethylene terephthalate) determined by d.s.c. *Polymer (Guildf)* 1978;19:1142–4. doi:10.1016/0032-3861(78)90060-5.

Chapter 4

4 Conclusions and Recommendations for Future Study

4.1 Conclusions

The bacterially-produced biopolymers poly(3-hydroxybutyrate) (PHB) and its copolymer poly(3-hydroxybutyrate-co-3-hydroxyhexanoate) (PHBH) are more environmentally-friendly in production than synthetic polymers,. Compared to PHB, PHBH has broader process temperature and higher ductility, but lower modulus and strength. Consequently, the main objective of this study was to develop PHBH composites with a wide range of mechanical properties using industry-friendly polymer processing equipment. Glass fiber (GF) and thermoplastic elastomers (TE) were used to, respectively, reinforce PHBH and to toughen glass fiber reinforced PHBH composites.

First, the effects of glass fiber on the mechanical and thermal properties of PHBH were investigated. PHBH composites were prepared by melt-compounding and injection molding, using PHBH with 3-hydroxyhexanoate (3HH) molar fractions of 5.6 and 11.1%, and short glass fiber content varying from 0 to 23 volume percent. Tensile test results suggested that the glass fiber addition significantly increased Young's modulus and strength of PHBH. The Halpin-Tsai and Tsai-Pagano equations were used to predict Young's modulus of PHBH composites while the modified Kelly-Tyson model with the Bowyer-Bader method were used for strength prediction. These predictions gave reasonable estimates for the mechanical properties of PHBH composites. Differential

scanning calorimetry results suggested that glass fiber addition had little effect on the degree of crystallinity of PHBH, as well as on the crystallization half-time of PHBH containing 5.6 mol% 3HH.

Although the addition of glass fibers is an effective method for improving both Young's modulus and tensile strength of PHBH, the addition of glass fibers reduced ductility and energy absorbed in fracture of PHBH. To increase ductility and/or energy absorbed in fracture of glass fiber reinforced PHBH composites, thermoplastic elastomers were added. The thermoplastic elastomers used were styrene-ethylene-butylene-styrene copolymer (SEBS) and maleated styrene-ethylene-butylene-styrene copolymer (SEBS-MA). Composites were prepared by melt-compounding and injection molding. Mechanical test results suggested that SEBS-MA was more effective than SEBS in improving ductility, fracture energy, and notched Izod impact strength of glass fiber reinforced PHBH composites. Scanning electron microscopy results suggested that SEBS-MA encapsulated fibers as well as dispersed in the PHBH matrix, whereas SEBS dispersed in the PHBH matrix without fiber encapsulation. Differential scanning calorimetry results suggested that both SEBS and SEBS-MA addition decreased the degree of crystallinity of glass fiber reinforced PHBH composites.

In conclusion, mechanical properties of PHBH can be tailored by the addition of glass fibers and thermoplastic elastomers; therefore, modulus, strength, and energy absorption in fracture of PHBH composites can be balanced. PHBH/GF composites may be suitable for applications where high stiffness and strength are required, whereas PHBH/GF/TE hybrid composites may be suitable for applications where energy absorption is more

important. The versatility of PHBH composites suggests that PHBH-based composite materials have many potential applications.

4.2 Recommendations for Future Study

The recommended future studies are described as follows:

- (1) This study showed that the addition of glass fiber increased Young's modulus and strength of PHBH. Although glass fibers have good mechanical properties, they are synthetic fibers and non-biodegradable. Using natural fibers, biodegradable natural fiber reinforced PHBH biocomposites can be developed. Furthermore, since natural fibers are lighter than glass fibers, the composites will be lightweight materials. However, natural fibers are susceptible to thermal degradation, absorb moisture, and have uncontrolled size. These complexities will require in-depth study.
- (2) This study also showed that the energy absorption capability of PHBH/GF composites can be increased by adding thermoplastic elastomers. It will be beneficial to study whether other types of elastomers can also increase energy absorption in fracture of PHBH/GF composites. Additionally, natural rubbers can be used to create greener composites.
- (3) Using nanofillers such as nanoplates, nanofibers, and nanotubes, PHBH nanocomposites can be developed. It has been reported that the addition of nanofillers can improve modulus and strength of various polymers. Typically, the

amount of nanofillers added is much smaller than that of conventional glass, carbon, or aramid fibers. Therefore, the addition of nanofillers may be able to improve modulus and strength of PHBH without sacrificing much ductility and energy absorption in fracture.

- (4) Numerical methods such as Finite Element Analysis (FEA) can be used to predict mechanical properties. This approach would also give better understanding of reinforcement mechanisms of fibers and would allow for simulation of mechanical properties when material parameters, such as matrix and fiber properties, fiber size, fiber geometry, and fiber volume fraction, are different.

Curriculum Vitae

Name: Willson Arifin

Post-secondary Education and Degrees: University of Wisconsin - Platteville
Platteville, Wisconsin, USA
2007-2011 B.Sc.

The University of Western Ontario
London, Ontario, Canada
2013-2015, MEd.

Related Work Experience Teaching Assistant
The University of Western Ontario
2013-2015

Research Assistant
The University of Western Ontario
2013-2015

Publications:

Arifin W, Kuboki T. (2015). Effect of Glass Fiber on Mechanical Properties of Poly(3-hydroxybutyrate-co-3-hydroxyhexanoate). Annual Technical Conference 2015 of Society of Plastics Engineers, Orlando, Florida, USA.